University of Nottingham
UK | CHINA | MALAYSIA

Optimising Biochar Preparation via Biomass Pyrolysis and Activation for Biomedical Application

by

Ke Cui

Thesis submitted to the University of Nottingham

for the degree of Master of Research

September, 2024

ABSTRACT

As a multifunctional material, biochar is widely used in environmental remediation, agricultural enhancement, energy storage, and more recently, has shown great potential in the medical field. Biochar's unique physical and chemical characteristics make it an attractive candidate for medical applications due to its large specific surface area, high porosity, and surface activity. However, current research on biochar's adsorption capacity in medical applications remains limited, particularly regarding how to optimise specific surface area and adsorption properties through controlled pyrolysis and activation processes. Thus, further research and optimisation are necessary.

Five representative biomass materials – poplar wood, bamboo slice, coconut shell, peanut shell, and rice straw – were selected as research subjects due to their distinct structural characteristics and economic viability. Significant variations in lignocellulosic composition were observed: cellulose and lignin predominated in poplar wood, cellulose constituted the primary component in bamboo slice, while rice straw was distinguished by its elevated ash content. Coconut shell was characterised by high carbon concentration and intrinsic porosity, whereas peanut shell and rice straw fragments demonstrated advantages in resource availability, cost-effectiveness, and collection feasibility. This diversified material selection facilitates a mechanistic understanding of how biomass compositional variations affect pyrolysis kinetics and biochar pore architecture. Five types of biomass were subjected to pyrolysis, and the KOH activation process further improved the pore structure and specific surface area of the biochar. The effects of temperature, raw material type, and activator on pore structure were investigated. The chemical composition, surface morphology, functional groups, and specific surface area of the biochar were characterised using thermogravimetric analysis (TGA), lignocellulose content determination, elemental analysis, Fourier-transform infrared spectroscopy (FTIR), scanning electron microscopy (SEM), and Brunauer–Emmett–Teller (BET) surface area analysis. Additionally, the relationship between the specific surface area of biochar, pyrolysis

parameters, and raw material type was systematically analysed.

The lignocellulose content analysis revealed that the cellulose content of poplar wood and coconut shell reached 51.36% and 51%, respectively, while the cellulose content of rice straw was significantly lower. These differences contribute to variations in volatile release and the specific surface area of different biomass types during pyrolysis. Elemental analysis showed that the H/C ratio of biochar decreased significantly with increasing pyrolysis temperature, indicating a transition from hydrocarbon structures to more stable aromatic carbon structures. Simultaneously, the decrease in the O/C ratio reflects reduced polarity in the biochar, which enhances its antioxidant properties. Ash content increased with temperature, potentially clogging pores and negatively affecting surface area. FTIR analysis demonstrated a significant reduction in hydroxyl (-OH) and carbonyl (C=O) groups in the biochar, forming more stable aromatic compounds. Additionally, the surface functional groups of AKP800 biochar, produced by KOH activation, were further enhanced. BET analysis revealed that poplar wood biochar prepared at 800℃ exhibited a higher specific surface area of 451.06 m^2/g. Under different activation conditions, the specific surface area of biochar (AKP800 and BKP800) was 2028.96 m^2/g and 1042.86 m^2/g, respectively, which is much larger than the values reported by other researchers. SEM observations showed that, under the combined effects of high-temperature pyrolysis and KOH activation, the porous structure of the biochar became more pronounced, offering favourable conditions for its application in medical adsorption.

This study revealed the effects of biomass chemical composition, pyrolysis conditions, and activation processes on the specific surface area and adsorption properties of biochar. Biomass with high cellulose and lignin content demonstrated a higher specific surface area during pyrolysis, and KOH activation further enhanced the porosity and specific surface area of the biochar, resulting in stronger adsorption properties. The biochar produced exhibited a significantly higher specific surface area compared to

those available on the market, indicating substantial potential for medical applications.

Keywords: biochar; KOH activation; pyrolysis; specific surface area; medical applications

ACKNOWLEDGEMENTS

My sincerest thanks go out to everyone who has supported and mentored me throughout this year. Their invaluable advice and knowledge have not only enriched my experience but also helped me overcome numerous challenges.

First and foremost, I want to express my deepest thanks to my mentor, Professor Cheng Heng Pang. His generosity in sharing his expertise and his dedication to fostering my skills have been truly inspiring. His patient guidance during every group meeting has been instrumental in helping me complete my master's thesis, while his life advice has also given me a clearer direction for my future.

I am equally grateful to my PhD friends, whose assistance in the lab, especially with solving technical problems, has been indispensable. The University of Nottingham Ningbo has provided an incredible platform, and for that, I am truly thankful. My time here has been filled with unexpected opportunities, and this year of research has contributed greatly to my personal growth.

Finally, I owe immense gratitude to my girlfriend and parents for their relentless support and motivation. Their confidence in me was crucial to my academic success.

TABLE OF CONTENT

ABSTRACT I

ACKNOWLEDGEMENTS IV

TABLE OF CONTENT V

LIST OF FIGURES VIII

LIST OF TABLES X

1. INTRODUCTION 1

1.1 Background 1

1.2 Biomass species 1

1.3 The origin and application of biochar 2

1.4 Purpose of research 4

2. LITERATURE REVIEW 6

2.1 Introduction of pyrolysis 6

2.2 Introduction and production of biochar 7

2.2.1 Chemical component of biochar 8

2.2.2 Process parameters and biochar production 8

2.2.3 Effects of temperature and feedstocks on biochar properties 11

2.3 Application of biochar 15

2.3.1 Biosensors and Detection 15

2.3.2 Drug delivery 16

2.4 Challenges of biochar application 17

3. EXPERIMENTAL 19

3.1 Experimental materials and chemicals 19

3.2 Experimental methods 20

3.2.1 Experimental process 20

3.2.2 Pretreatment of biomass samples 21

3.2.3 Pyrolysis experiments of biomass and activated biomass 22
3.3 Characterisation of biochar 23
3.3.1 Thermogravimetric experiment (TGA).....23
3.3.2 Determination of lignocellulose (CHL).....24
3.3.3 Ash content determination 25
3.3.4 Determination of elemental content.....25
3.3.5 Fourier transform infrared spectroscopy (FT-IR) 25
3.3.6 Scanning electron microscopy (SEM) 26
3.3.7 Determination of specific surface area (BET) 27
4. RESULTS AND DISCUSSION.....29
4.1 Introduction 29
4.2 Properties of biomass 29
4.2.1 Thermogravimetric analysis (TGA).....29
4.2.2 Elemental analysis of biomass.....32
4.2.3 Analysis of lignocellulose content 33
4.3 Properties of biochar 35
4.3.1 Biochar yield.....35
4.3.2 Ash content of biochar 36
4.3.3 Elemental analysis of biochar 37
4.3.4 Fourier transform infrared spectrum of biochar (FT-IR) 41
4.3.5 Scanning electron microscopy of biochar (SEM).....46
4.3.6 Specific surface area analysis of biochar (BET).....49
4.4 Properties of activated samples 53
4.4.1 Fourier transform infrared spectrum of activated biochar (FT-IR).....53
4.4.2 Scanning electron microscopy of activated biochar (SEM) 55
4.4.3 Specific surface area of activated biochar (BET) 56
4.5 Relationship between temperature, lignocellulose and specific surface area 61
5. CONCLUSIONS AND PROSPECT 64

REFERENCES 66

LIST OF FIGURES

Figure 1.1 The pyrolysis process of this experiment. 5
Figure 2.1 The influence of pyrolysis temperature on biochar structure: a) amorphous carbon; b) turbostratic carbon; c) graphite carbon[48]. 13
Figure 2.2 Applications of biochar in different fields[60]. 15
Figure 2.3 Medical application of biochar[22]. 17
Figure 3.1 The research process of this experiment. 21
Figure 3.2 Image of pyrolysis equipment. 23
Figure 3.3 Image of the TGA instrument. 24
Figure 3.4 Image of the FTIR instrument. 26
Figure 3.5 SEM equipment (left) and EDS instruments (right). 27
Figure 3.6 Image of the BET instrument. 28
Figure 4.1 The yield of biochar prepared at different pyrolysis temperature. 35
Figure 4.2 Ash content of biological carbon prepared at different pyrolysis temperatures. 36
Figure 4.3 Elemental composition of organic components of different biochar at different temperatures. 41
Figure 4.4 Fourier transform infrared spectrum of PW500-PW900. 43
Figure 4.5 Fourier transform infrared spectra of CS500-CS900. 44
Figure 4.6 Fourier transform infrared spectra of BS500-BS900. 44
Figure 4.7 Fourier transform infrared spectra of PS500-PS900. 45
Figure 4.8 Fourier transform infrared spectra of RS500-RS900. 45
Figure 4.9 SEM images of (a) PW500, (b)PW600, (c)PW700, (d)PW800, (e)PW900. 47
Figure 4.10 SEM images of (a) CS500, (b)CS600, (c)CS700, (d)CS800, (e)CS900. 47
Figure 4.11 SEM images of (a) BS500, (b)BS600, (c)BS700, (d)BS800, (e)BS900. 48
Figure 4.12 SEM images of (a) PS500, (b)PS600, (c)PS700, (d)PS800, (e)PS900.

.....48
Figure 4.13 SEM images of (a) RS500, (b)RS600, (c)RS700, (d)RS800, (e)RS900.
.....49
Figure 4.14 FTIR spectra of poplar biochar activated from KOH.....55
Figure 4.15 SEM images of (a) AKP800, (b)BKP800.....56
Figure 4.16 N_2 adsorption-desorption isotherm of biochar AKP800 and BKP800.
.....58
Figure 4.17 Pore size distribution of biochar AKP800 and BKP800 by DFT model.
.....58
Figure 4.18 Types of physical adsorption isotherms (a) and types of desorption hysteresis loops (b)[103].....59
Figure 4.19 The specific surface area of biochar produced by each biomass at different.....62
Figure 4.20 The relationship between the content of cellulose and the specific surface area of biochar prepared at different pyrolysis temperatures. 63

LIST OF TABLES

Table 2.1 Main process types and conditions of biomass pyrolysis[27].....6
Table 2.2 Biochar production efficiency of different methods[34].....9
Table 2.3 Cellulose, hemicellulose, and lignin contents in lignocellulosic material (%)[42].....10
Table 2.4 Properties of biochar prepared from diverse biomass raw materials....12
Table 3.1 A concise expression of the biomass name 19
Table 3.2 Information of Chemicals in the Experiments 20
Table 4.1 Proximate analysis of samples (%) 32
Table 4.2 Ultimate analysis of biomass (%) 33
Table 4.3 Content of lignocellulose in different biomass (%) 34
Table 4.4 Ultimate analysis biochar (%) and atomic ratio [H/C, O/C, (N+O)/C] 39
Table 4.5 Pore parameters of biochar 52
Table 4.6 EDS analysis of activated biochar 56
Table 4.7 Pore parameters of activated biochar.....61

1. INTRODUCTION

1.1 Background

Biochar, a porous carbon material produced by high-temperature pyrolysis of biomass under hypoxic conditions, has recently attracted significant attention in the medical field. Biochar exhibits significant promise in medical applications owing to its distinct physical and chemical characteristics, including high stability, a porous framework, excellent biocompatibility, and remarkable adsorption capabilities. Its superior adsorption performance is primarily due to its vast surface area and numerous active sites. Furthermore, biochar serves as a catalyst in various reactions through the generation of persistent free radicals (PFR). Its porous nature and expansive surface area allow for the integration of diverse functional chemicals, making it a versatile carrier for a wide range of uses[1]. Biochar's versatility has made it a prominent material in medical research and applications, from drug carriers to tissue-engineered scaffolds, wound dressings, and biosensors. As biochar research continues to evolve, it is critical to understand its interactions with biological systems and optimise its performance for medical applications.

1.2 Biomass species

Biomass is considered environmentally friendly because it does not contribute to a net increase in atmospheric CO_2 emissions. The CO_2 released when biomass is used as energy equals the CO_2 absorbed during plant photosynthesis[2]. A variety of natural and processed materials serve as biomass resources for production, including woody and herbaceous plants, wood waste, agricultural and industrial residues, paper, municipal solid waste, biosolids, food processing waste, animal manure, aquatic plants, and algae[3]. This study focuses on woody and herbaceous biomass, consisting primarily of organic compounds like cellulose, hemicellulose, and lignin, along with smaller amounts of proteins, fats, and inorganic substances. The structure and composition of these organic materials determine their energy properties and

conversion efficiency.

Cellulose, hemicellulose, and lignin, also known as lignocellulose, degrade slowly in biomass[4]. The cell wall structure of biomass primarily consists of these three polymers. Typically, the composition of biomass includes cellulose (30%-50%), hemicellulose (14%-25%), and lignin (15%-35%)[5]. The proportions and interactions of these polysaccharides vary depending on the type of biomass, plant species, and even the biomass source[6].

Various processes have been developed to utilise biomass for energy production efficiently. Among biomass conversion technologies, pyrolysis is widely regarded as advantageous due to its flexibility in generating solid biochar and liquid bio-oil from raw materials[7]. Biomass pyrolysis involves processing biomass at high temperatures, and it includes several methods: slow pyrolysis, fast pyrolysis, and flash pyrolysis. Slow pyrolysis, a thermochemical decomposition under limited oxygen, is recognised as a suitable process for producing biochar, resulting in stable carbon, a uniform structure, and a high yield[8].

1.3 The origin and application of biochar

Biochar is a black carbon material formed through the incomplete combustion or pyrolysis of biomass. It can be produced naturally, such as through forest fires, straw burning, or human activities. Historically, biochar was discovered by ancient Amerindian inhabitants of the Amazon region and is often referred to as Terra Preta de Indio[9]. This black carbon-rich soil is highly fertile and contains significant amounts of carbon. In 2007, Lehmann proposed using modern cryogenic pyrolysis technology to convert biomass into biochar. In 2010, Woolf et al. systematically elaborated the concept of sustainable biochar[10]. Since then, more scholars have evaluated the potential of biochar for soil improvement and carbon sequestration.

Biochar is highly aromatised and resistant to decomposition. It has various applications, including solid fuel, functional filler in polymer materials, catalyst substrate, absorbent, and soil amendment[11]. Different applications require biochar with specific properties. Earlier studies have provided detailed insights into how variations in pyrolysis conditions, such as maximum treatment temperature, heating rate, and residence time, impact biochar yield and properties[12]. Additionally, researchers have characterised biochar produced from various types of biomass. Their findings show that biomass composition and pyrolysis temperature significantly impact biochar properties. For instance, high temperatures, low pressure, and high heating rates during pyrolysis produce biochar with higher carbon content and a larger specific surface area[13]. Its porous structure and large surface area make it an effective carrier for functional chemicals. In addition, biochar shows easy modification in terms of raw material composition, chemical structure, porosity, functional groups, and specific surface area[14], making its performance even better. Modification techniques include physical methods for optimising properties and chemical activation using acidic or alkaline agents[15].

In recent years, biochar has been widely applied in various fields. Examples include nutrient recovery[16], soil improvement, waste water treatment[17], and energy production[18], all of which address issues that have more or less an indirect or indirect impact on human health. For instance, heavy metal contamination in water poses a significant threat to human health, potentially causing damage to the stomach, lungs, and liver[19]. The high adsorption of biochar can effectively remove heavy metals from wastewater, as well as other toxic elements (PTE) [20]and triclosan (TCS)[21].

In conclusion, biochar has a significant connection to human health. In recent years, it has gained increasing attention in the medical field, expanding its potential applications and practicality. Currently, biochar is employed in five significant medical applications: immobilizing pollutants, treating medical waste and recovering nutrients, evaluating its

toxicity, developing electrical sensors and biosensors, and enhancing drug delivery systems[22]. Studies have shown that biochar outperforms other drug carriers in terms of quality. A comprehensive comparison between biochar and other nanocarriers in drug delivery systems has been explored in depth for the first time. Furthermore, research indicates that biochar could be used to treat diseases requiring regular, long-term administration. The use of biochar in medicine is an emerging field, with some areas still in their early stages but showing significant potential for future development.

1.4 Purpose of research

Understanding the relationship between biochar and medical treatment relies on its structure, as well as its physical and chemical properties. For instance, when using biochar as a soil amendment, factors such as pH, cation exchange capacity, and porosity must be considered[23]. In the context of soil and water pollution remediation, adsorption mechanisms play a key role[24]. When applying biochar in the medical field, its specific surface area becomes critical. In physical adsorption, it is important to develop the specific surface area of biochar. In chemisorption, the presence of functional groups capable of binding contaminants is paramount. Therefore, selecting carbon materials with appropriate properties is crucial.

Currently, extensive research focuses on the characteristics and specific surface area of biochar, but the precise effects and advantages of each component on the specific surface area of biochar remain somewhat unclear. Understanding the correlation between the chemical composition of biomass and the specific surface area of biochar is still challenging. It requires further investigation, as the chemical composition and structure of biomass vary significantly and cannot be artificially controlled.

In this study, biochar was produced from poplar wood, bamboo slices, coconut shells, peanut shells and rice straws. Biochar was modified by controlling production factors, such as pyrolysis conditions (type of raw material and temperature) and chemical

activation. Through thermogravimetry analysis (TGA), Fourier-transform infrared spectroscopy (FTIR), scanning electron microscopy (SEM), and specific surface area measurement (BET), the changes in surface properties were analysed, including surface area, surface morphology, functional groups, and elemental content distribution. The biochar with the best performance was selected, and its raw materials were chemically activated at the optimal temperature. A characterisation experiment was conducted to determine whether the properties of the activated biochar had improved. By comparing our results with those of previous studies, we will demonstrate that our biochar offers distinct advantages. The objective of this study is to select appropriate biomass and apply optimal pyrolysis and activation conditions to produce biochar with enhanced performance and greater potential. Figure 1.1 shows the pyrolysis process of this experiment.

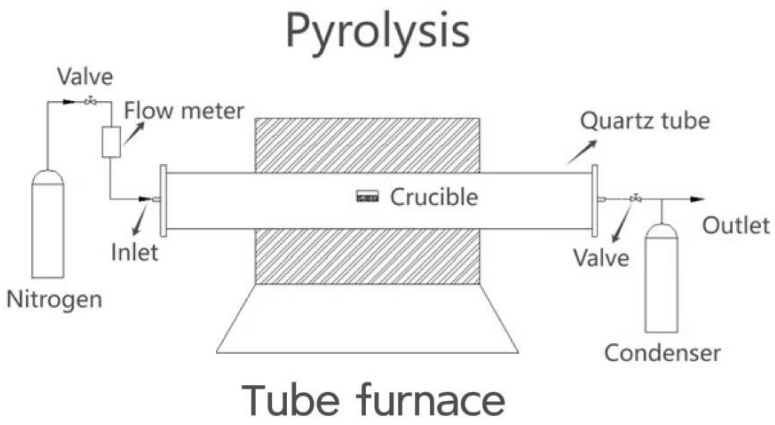

Figure 1.1 The pyrolysis process of this experiment.

2. LITERATURE REVIEW

2.1 Introduction of pyrolysis

In biomass pyrolysis, biomass is decomposed in an inert environment between 300°C and 1000°C, resulting in bio-oil, biochar, and pyrolysis gas[25]. A pyrolytic reaction generally consists of two stages: pyrolysis primary and pyrolysis secondary. The primary phase of biomass processing involves the dehydration, the decarboxylation, and the dehydrogenation of volatile substances to form carbonyl, carboxyl, and hydroxyl groups. Biochar or biogas are produced from secondary pyrolysis of biomass. The pyrolysis products derived from cellulose and hemicellulose are predominantly volatile substances, while biochar is mainly produced from the pyrolysis of lignin[26].

Pyrolysis is classified based on operational factors such as temperature, heating pace, and duration. The main types include conventional pyrolysis, microwave pyrolysis, catalytic pyrolysis, hydrothermal pyrolysis, and hydrogenation pyrolysis. Conventional pyrolysis could be further divided into fast pyrolysis, slow pyrolysis, and flash pyrolysis (Table 2.1).

Table 2.1 Main process types and conditions of biomass pyrolysis[27]

Thermochemical Conversions	Residence Time	Heating Rate (℃/s)	Temperature (℃)	Major Product
Slow Pyrolysis	> 0.5h	0.01-2	< 450	Biochar
Fast Pyrolysis	0.5-5 s	100-1000	450-600	Biooil
Flash Pyrolysis	< 1 s	> 1000	> 450	Biooil

Slow pyrolysis is a process that subjects solid biomass fuel to high temperatures for extended periods, allowing for thorough volatilisation and carbon generation, whose typical characteristics include a slow heating rate, prolonged carbonisation time, and limited aeration to reduce oxidation losses of the raw materials. The slow pyrolysis process has evolved from primitive pile charcoal burning and carbonisation kilns to advanced technologies such as continuous multi-layer carbonisation furnaces and

internally heated vertical retorts used in large-scale industrial production[28]. Several factors influence the product distribution and composition, including the type and size of the raw materials, reaction temperature, pressure, and the residence time of solids and volatiles[29]. Optimising these parameters is crucial for improving the efficiency and yield of desired products.

Fast pyrolysis is a thermochemical process in which biomass fuel undergoes rapid thermal decomposition and condensation with oxygen-free, which primarily converts biomass into liquid products, commonly referred to as biomass pyrolysis liquefaction. Fast pyrolysis is typically conducted at atmospheric pressure and moderate temperatures, creating relatively mild process conditions. The resultant liquid product, known as bio-oil or pyrolysis oil, could be utilised as a fuel. Benefiting from its ease of storage and transport, bio-oil holds the potential to replace petroleum, raising significant attention. Biomass-fast pyrolysis reactors are classified into several types, including bubbling fluidised bed, circulating transfer bed, circulating fluidised bed reactor, ablation reactor, rotating cone reactor, and vacuum moving bed reactor[30].

2.2 Introduction and production of biochar

Biochar is a carbon-rich, stable product resulting from the high-temperature pyrolysis of biomass in oxygen-free or limited aeration[31]. Its properties include an extensive specific surface area, a highly developed microporous framework, and numerous oxygen-containing functional groups. These properties enable biochar to adsorb nutrients, metal ions, and organic compounds from the soil. The ability of biochar to immobilise nutrients and pollutants helps to control pollutant migration, thereby mitigating environmental pollution. Additionally, the biochar can likewise be used to boost soil top quality, and promote plant development and thus enhance dirt fertility. Besides, biochar likewise plays an essential function in carbon and nitrogen sequestration, which can help in reducing greenhouse gas emissions[32].

2.2.1 Chemical component of biochar

Biochar is a strong product produced by biomass pyrolysis with a high carbon material, varying from 65% to 90%. It normally looks black, fluffy, and strong, composed largely of aromatic hydrocarbons and single carbon or carbon with a graphitic-like structure. The elemental structure of biochar usually includes carbon (C), hydrogen (H), and oxygen (O), as well as trace elements such as nitrogen (N), sulphur (S), phosphorus (P), potassium (K), calcium (Ca), magnesium (Mg), sodium (Na) and silicon (Si). Carbon is the greatest component, commonly over 60%, complied with by hydrogen and oxygen, while mineral elements are primarily discovered in ash products[33]. The carbon in biochar is mostly in the form of fragrant carbon, arranged in uneven heaps of secure aromatic rings. Nitrogen is mainly present externally in biochar in the form of a C-N heterocyclic framework. The phosphorus material in biochar is reasonably reduced and differs greatly, which is adversely associated with pyrolysis temperature. This irregularity might be connected to the high pH produced during the carbonisation procedure and the formation of phosphates, including components such as calcium and magnesium. The focus of potassium, calcium, magnesium, and salt varies in various sorts of biochar. For example, biochar from livestock and poultry manures generally contains the highest levels of these minerals, followed by herbaceous plant biochar, with woody plant biochar having the lowest mineral contents.

2.2.2 Process parameters and biochar production

Biochar is the production of thermochemical conversion of biomass using methodologies including pyrolysis, torrefaction, gasification, and hydrothermal carbonisation, as mentioned above. Suitable technology and optimisation of conditions such as temperature, residence time, heating rate, and reaction environment are essential for efficient biochar production. Among these methods, slow pyrolysis stands out due to its slow heating rate and long residence time, which can maximise the yield of solid biochar. Table 2.2 illustrates the characteristics of various thermochemical processes and the typical yield of biochar for each method, which can help adjust process parameters to improve biochar production efficiency and yield.

Table 2.2 Biochar production efficiency of different methods[34]

Thermochemical Conversions	Residence Time (s)	Heating Rate (℃/min)	Temperature (℃)	Biochar Production (%)
Slow Pyrolysis	> 3600	5-7	~ 300	35-50
Fast Pyrolysis	0.5-10	300-800	450-600	15-35
Flash Pyrolysis	< 1	~ 1000	> 450	10-20
Gasification	10-20	3000-6000	600-1200	< 10
Hydrothermal Pyrolysis	> 300	5-10	180-260	45-70

The heating rate, temperature, and residence time significantly influence both the performance and yield of biochar. Temperature is the primary factor of operational characteristics[35]. As the temperature increases, the yield of biochar generally decreases, though the carbon content and surface area of the produced biochar enhance with rising temperature[36]. During the pyrolysis process, the degradation of biomass components occurs at distinct temperature ranges. For instance, hemicellulose decomposes between 220°C and 315°C, cellulose in a range between 315°C and 400°C, and lignin over a wider range of 160°C to 900°C[37].

An increased heating rate results in a secondary pyrolysis response, which subsequently reduces the biochar yield[38]. Conversely, a lower heating rate does not initiate secondary pyrolysis or cracking, leading to a higher biochar yield. Higher heating rates cause rapid evaporation and increased porosity, while a slower heating rate, such as $10℃\cdot min^{-1}$, facilitates the formation of a stable network post-decomposition, which accommodates the emission of volatile compounds[39]. Typically, the percentage of heating distribution and pyrolysis temperature are considered in conjunction with retention time. At the same pyrolysis temperature, the yield of biochar decreases as retention time increases[40]. Longer residence times at the heating temperature lead to

a reduction in the volatile matter of the biochar while the fixed carbon content increases[41].

In addition, the yield of biochar is also related to its raw materials. Cellulosic biomass is primarily composed of cellulose, hemicellulose, and lignin, with minor quantities of water-soluble extracts and ash. The relative proportions of cellulose, hemicellulose, and lignin in biomass can vary significantly depending on the specific materials (shown in Table 2.3). Straw biochar, for instance, exhibits a higher volatile content, which is more readily expelled during pyrolysis. Consequently, materials with elevated volatile content may lead to lower biochar yields.

Table 2.3 Cellulose, hemicellulose, and lignin contents in lignocellulosic material (%)[42]

Lignocellulosic material	Cellulose	Hemicellulose	Lignin
Hardwood stems	40-55	24-40	18-25
Coastal bermudagrass	25	35.7	6.4
Primary wastewater solids	8-15	-	-
Nut shells	25-30	25-30	30-40
Corn cobs	45	35	15
Switchgrass	45	31.4	12
Waste papers from chemical pulps	60-70	10-20	5-10
Solid cattle manure	1.6-4.7	1.4-3.3	2.7-5.7
Wheat straw	30	50	15
Grasses	25-40	35-50	10-30
Leaves	15-20	80-85	0
Softwood stems	45-50	25-35	25-35
Cotton seed hairs	80-95	5-20	0

At temperatures below 300°C, cellulose degradation primarily involves the disruption of intermolecular and intramolecular hydrogen bonds and the dehydration of hydroxyl groups. As the temperature increases, glycosidic bonds cleave, and some pyran rings decompose, leading to the formation of products such as oligosaccharides, acids, ketones, CO_2, and CO. Following dehydration, cellulose undergoes cross-linking reactions, ultimately resulting in the formation of biochar. The elevated mass loss rate of cellulose enhances the porous structure of the resulting pyrolysis biochar, while higher pyrolysis temperatures facilitate condensation and aromatisation within and between biochar molecules. Hemicellulose decomposes at temperatures below 250°C primarily through dehydration, decarboxylation, and the removal of unstable carbohydrate branches, producing CO_2. Lignin, a key precursor in biomass pyrolysis, has a highly aromatic structure that contributes to an increased yield of biochar.

2.2.3 Effects of temperature and feedstocks on biochar properties

The type of raw materials used significantly influences the physical and chemical properties of biochar[43]. Biochar produced from various raw materials exhibits distinct properties[44], with wood biochar generally demonstrating the greatest potential for surface area. Table 2.4 provides a summary of biochar properties derived from different biomass feedstocks.

Table 2.4 Properties of biochar prepared from diverse biomass raw materials

Feedstocks	Methods	C content (%)	Surface area (m^2/g)	Pore volume (cm^3/g)	Average pore size (nm)	Ref.
Poplar wood	Fast Pyrolysis, 350-600 ℃	69.9-93.1	208-416	0.08-0.17	0.2-1.4	[44]
Douglas fir wood		70.5-97.8	145-500	0.06-0.20		
Douglas fir bark		66.1-78.1	171-423	0.07-0.17		
Loblolly pine	Fast Pyrolysis, 300-1000 ℃	36.2-92.9	1.98-329.63	0.0004-0.0101	< 2	[45]
Pine cone	Slow Pyrolysis, 500 ℃	71.50	335	-	3.1	[46]
Wheat husk	500 ℃	50.50	63.8	-	-	[47]

As shown in Table 2.4, the properties of biochar are influenced by both the characteristics of raw materials and heating conditions. The fixed carbon content in biochar generally increases with rising pyrolysis temperatures. Higher pyrolysis temperatures reduce the release of carbon-rich compounds, while volatile compounds such as CO, CO_2, and HCN continue to be released, increasing the fixed carbon content of the remaining biochar.

In addition to biochar yield and fixed carbon content, specific surface area is a crucial parameter of biochar that is also affected by pyrolysis temperature. The influence of

pyrolysis temperature on the structure and functional groups of biochar is depicted in Figure 2.1. Biochar formed at elevated temperatures (600-700 °C) demonstrates a highly hydrophobic nature and well-organised carbon layers [48]. It is widely accepted that as carbonisation temperature increases, more volatile substances are released from the biomass surface, enhancing the aromatic carbon structure and nanopore size of the biochar. This process generates biochar with a larger surface and more pores, thereby boosting its adsorption efficiency.

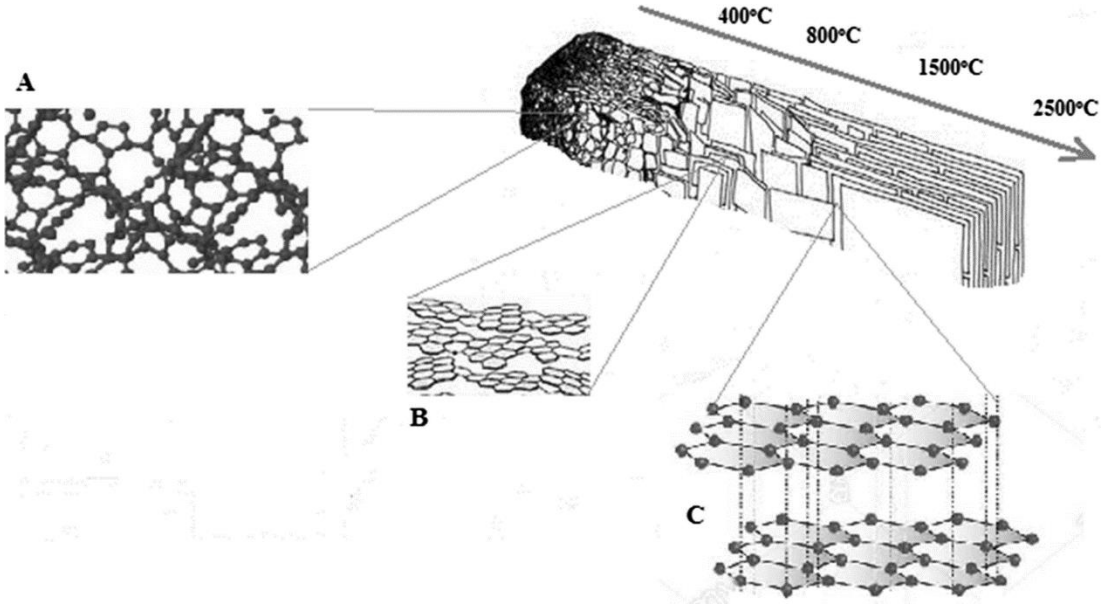

Figure 2.1 The influence of pyrolysis temperature on biochar structure: a) amorphous carbon; b) turbostratic carbon; c) graphite carbon[48].

On top of that, acid or base modification can also change the surface properties of biochar. On the one hand, acid-modified biochar is commonly functionalised via hydrochloric acid, sulfuric acid, etc., which could increase the diversity and density of carboxyl groups and oxygen-containing functional groups on the biochar surface. The modified surface could enrich its active sites and thus enhance its absorption rate through electrostatic interaction or functional group bonding. For example, the high sorption capacity of nitric acid-activated biochar for divalent copper ions could be attributed to its surface-layered structure and carboxyl groups[49]. On the other hand, acid treatment can promote the pore properties of biochar like both surface area and porosity. The acid removes impurities on the biochar surface, thereby upregulating the

number of micropores and mesopores within the biochar. Mahmoud et al. proved that post-acid treatment of kenaf fibre biochar with HCl can lead to an increase in BET surface area (from 289.497 m^2/g to 346.57 m^2/g), and SEM images demonstrated that the pores on the surface of kenaf fibre biochar after treatment present honeycomb-like gaps with different pore volume[50].

Similarly, alkali treatment could also contribute to the improvement of functional groups and pore properties of biochar. Alkali modification is generally carried out by potassium hydroxide or sodium hydroxide. The introduction of high-density oxygen-containing functional groups, such as alcohol and carboxyl groups, on the surface of NaOH-adjusted biochar switches the adsorption mechanism of biochar from physical adsorption (van der Waals force) to chemical one (surface complexation and ion exchange). Moreover, several studies have demonstrated the potassium hydroxide (KOH) modification leads to an increased surface area and micropore volume[51][52]. The underlying mechanism of porosity formation was explored via FTIR analysis, which revealed that the transformation from KOH to K_2CO_3 played a key role in the structure adjustment[53]. Besides, according to Galhetas et al., K_2CO_3, as a weak base, could also present the potential to modify biochar with an enhanced porosity[54]. In addition, biochar functionalised with another base (NaOH) illustrated a similar result with an enhanced surface area (932 m^2/g) and a strong microporous structure (with a pore volume of 0.42 cm^3/g)[52]. Briefly, the reaction mechanism of alkaline hydroxide (NaOH and KOH) treatment can be expressed as follows[53][55]:

$$2\,\mathrm{NaOH\,(KOH)} + CO_2 \rightarrow Na_2CO_3\,(K_2CO_3) + H_2O \quad (1)$$

$$2\,\mathrm{C} + 2\,\mathrm{NaOH\,(KOH)} \rightarrow 2\,\mathrm{CO} + 2\,\mathrm{Na\,(K)} + H_2 \quad (2)$$

$$Na_2CO_3\,(K_2CO_3) + \mathrm{C} \rightarrow Na_2O\,(K_2O) + 2\,\mathrm{CO} \quad (3)$$

$$Na_2O\,(K_2O) + \mathrm{C} \rightarrow 2\,\mathrm{CO} + 2\,\mathrm{Na\,(K)} \quad (4)$$

In conclusion, the physical and chemical residential or commercial properties of biochar are determined by its raw materials and pyrolysis parameters.

2.3 Application of biochar

Biochar has the attributes of alkaline, plentiful pore framework, large details surface area, strong adsorption capacity, low mass thickness, high stability, and high cost-effectiveness. Water and wastewater filtration, carbon sequestration, and natural waste adsorption are a few uses for it [56], electrochemical power storage space, and various other related areas. For example, Li et al. assessed the catalytic activity of biochar for tar removal and found that the enhancement of biochar dramatically minimised tar manufacturing compared to different biomass feedstocks[57]. Yousaf et al. explored the result of sawdust biochar on primary soil carbon mineralisation and discovered that it can substantially improve soil carbon storage space, so its improved carbon retention rate can be utilised as a practical method to improve dirt efficiency[58]. In addition, biochar is effective in binding organic pollutants including pesticides[59]. In recent years, biochar has also gained attention in the medical field due to its large specific surface area and other favorable physical and chemical properties. Beyond its use as an adsorption and removal agent for medical waste, biochar holds the potential to serve as drug delivery, biosensor, and tissue restoration and reconstruction materials.

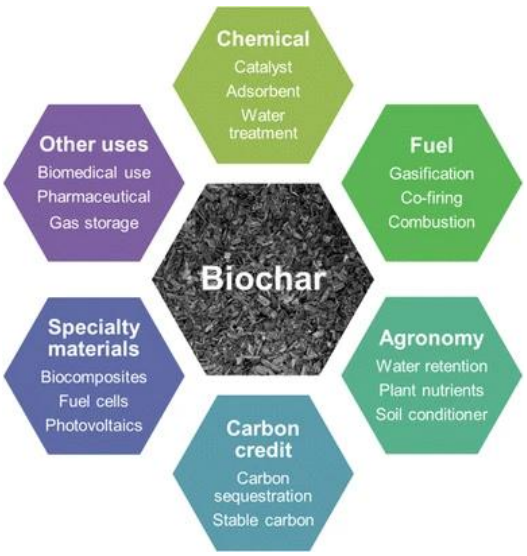

Figure 2.2 Applications of biochar in different fields[60].

2.3.1 Biosensors and Detection

The application of biochar as a biosensor in the medical field has been reported. In this

method, the target compound is first combined with biochar, and then the biochar transmits the electronic signal to a computer for accurate measurement. Dong et al. developed highly conductive and absorbent biochar nanoparticles for the detection of 17 β-estradiol in water. They found that the BCNP800 (generated at 800°C) exhibited the best absorption and conductivity with a limit of detection of 11.30 nm, showing comparable accuracy and reliability to conventional high-performance liquid chromatography[61]. In addition, biochar also acts as a catalyst, although the specific mechanism is not fully understood. Studies speculate that its morphology may play a key role in improving catalytic performance[62]. Taking advantage of this catalytic property, Kalinke et al. created a non-enzymatic biosensor to detect glucose levels in human saliva, achieving an excellent limit of detection (0.457 μm)[63]. Furthermore, biochar can be used as a carrier to load specific functional molecules due to its high surface area and abundant pore structure, thereby enhancing detection capabilities. For example, Cancelliere et al. employed biochar to fill an IL-6 antibody for the detection of IL-6 in human blood with a detection limitation of 4.8 pg/ml and revealed higher sensitivity and reproducibility than conventional ELISA package[64].

2.3.2 Drug delivery

Biochar's porous framework and big surface area make it an excellent drug carrier. In addition, the intrinsic buildings of biochar permit it to be easily modified for particular functionalization, consisting of targeted delivery and stimulus-responsive launch. Compared with nanocarriers that that are widely studied in current drug delivery systems, biochar has numerous advantages, consisting of an easy synthesis procedure, affordable, long-lasting security, and simplicity of functionalization.

Wang et al. created a medication shipment system using hydrogel spheroids doped with ZnO functionalised biochar[65]. The enhancement of the modified biochar allows slow and continual drug launch, light-controlled medication distribution, and potential antimicrobial impacts. The safety evaluation results showed that the compound had no evident poisoning in vitro or in vivo. Designed for subconjunctival implantation, this

advanced medicine distribution system makes it possible for stable and long-lasting drug release for as many as 17 days, getting rid of the need for constant dosing. This addresses the substantial challenge of repeated administration in glaucoma therapy. This study shows the prospective application worth of biochar in the therapy of glaucoma and reveals the pledge of biochar in the therapy of various other illnesses that call for repeated application, such as diabetic issues and high blood pressure.

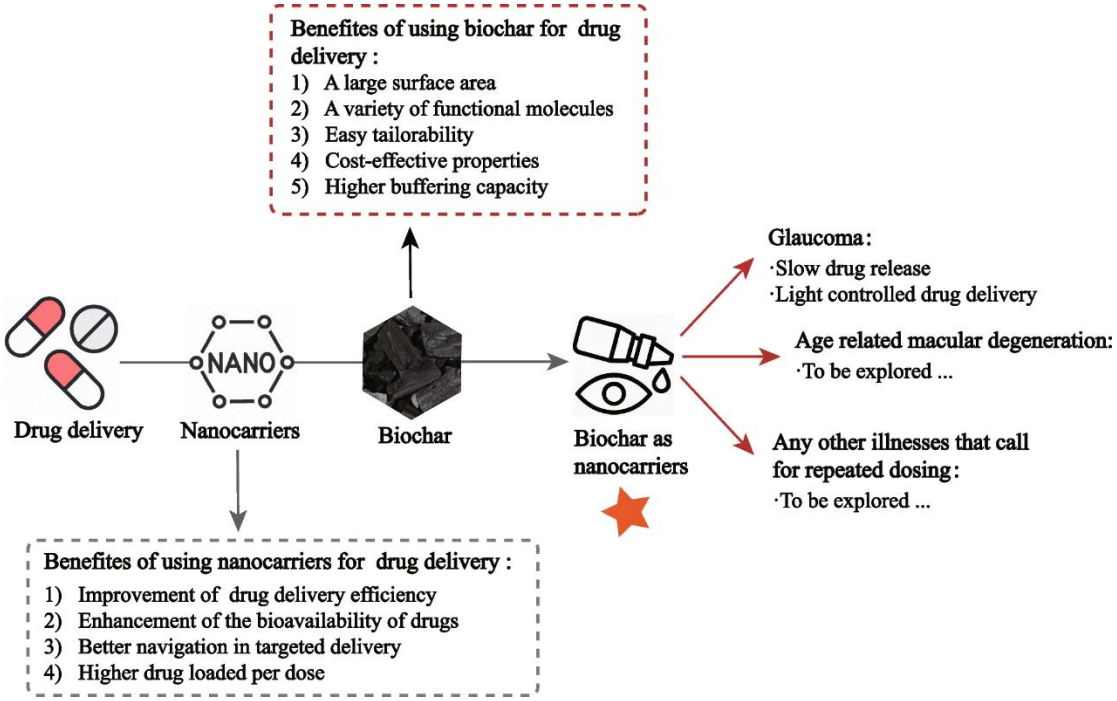

Figure 2.3 Medical application of biochar[22].

2.4 Challenges of biochar application

Although biochar has demonstrated potential in the clinical field, research in this area is still in its early stages. Due to the limited number of relevant studies, several challenges remain in the medical application of biochar. First, the porous structure of biochar is beneficial for medical applications. While high pyrolysis temperatures promote the formation of this structure, excessively high temperatures may reduce its functionality. However, the specific impact of elevated temperatures has not been extensively studied. Additionally, the pore structure and specific surface area of biochar are closely related to its adsorption capacity. However, studies have not adequately explored the relationship between specific surface area and biomass composition.

Furthermore, biochar with an optimally large specific surface area has yet to be developed, which remains a critical challenge for its use in medical applications.

Additionally, certain applications, such as drug delivery systems, present challenges related to safety performance. Since these systems come into direct contact with the human body, considerations such as safety, toxicity, immunogenicity, and degradation products are critical. As a result, their development must be approached with caution and often incurs relatively high costs.

In conclusion, the research on biochar in this paper can begin with the following aspects: (1) Investigating pyrolysis temperatures between 500℃ and 900℃ to determine the optimal temperature for producing biochar with the largest surface area. (2) Comparing the relationship between the lignocellulose content and the specific surface area of the biomass used in the experiment to identify which components of the raw material have the greatest impact on surface area. (3) Activating and pyrolysing the biomass with the best performance in the experiment to produce biochar with a more advantageous surface area compared to previous studies.

3. EXPERIMENTAL

3.1 Experimental materials and chemicals

This study selected poplar wood, coconut shells, peanut shells, bamboo slices, and rice straw as research materials, each with distinct characteristics. The high levels of cellulose and lignin in poplar wood result in biochar with a high specific surface area and a stable carbon structure. Coconut shells and bamboo pieces have been widely studied in biochar preparation. Coconut shells are rich in lignocellulose, with low mineral content in their biochar, which gives them excellent adsorption properties. Bamboo is also rich in lignocellulose, grows rapidly, and is renewable. Peanut shells provide a good foundation for biochar adsorption and offer significant utilisation potential. Rice straw, due to its low cost and abundant availability, helps reduce production costs. These materials were selected for this experiment. To express them concisely, this study will abbreviate their names. Table 3.1 provides a summary of the biomass names.

Table 3.1 A concise expression of the biomass name

Biomass	Abbreviation
Poplar Wood	PW
Bamboo Slice	BS
Coconut Shell	CS
Peanut Shell	PS
Rice Straw	RS

In this study, 65-mesh screen was used to reduce the biomass particle size to less than 230 μm, increasing the contact area during the reaction process. Table 3.2 presents the chemical information used in the experiment. Deionized water was used for testing.

Table 3.2 Information of Chemicals in the Experiments

Chemical name	Purity	Manufacturer	Solution preparation
Sulfuric Acid (H_2SO_4)	AR	National Group Chemical Reagent Co., LTD	Measure 5.75 and 120ml of concentrated H_2SO_4, add water to 200ml, and configure 5 and 72% H_2SO_4 respectively
Potassium Hydroxide (KOH)	AR	National Group Chemical Reagent Co., LTD	Measure 48g of KOH solids, mix with 152.16ml of water, and configure 24% KOH
Acetone	AR	National Group Chemical Reagent Co., LTD	Measure 175.5ml acetone solution
Absolute Ethyl Alcohol	AR	National Group Chemical Reagent Co., LTD	Measure 315ml anhydrous ethanol solution

3.2 Experimental methods

3.2.1 Experimental process

The entire experimental procedure is illustrated in the figure 3.1. Five types of biomass were subjected to pyrolysis at varying temperatures to generate biochar. Subsequently, a series of characterisation techniques were employed to analyse the biochar, providing a comprehensive understanding of its physical and chemical properties. These techniques encompassed thermogravimetric analysis (TGA), lignin cellulose (CHL), ash content, elemental analysis, Fourier transform infrared spectroscopy (FTIR), scanning electron microscopy (SEM), and specific surface area (BET) measurements. Following the initial characterisation, the biomass exhibiting superior performance was selected, activated, and subsequently pyrolysed at the optimal temperature. The biochar was further characterised through Fourier transform infrared spectroscopy (FTIR), scanning electron microscopy-energy dispersive X-ray spectroscopy (SEM-EDS), and

specific surface area (BET) measurements. Subsequently, the relationship among temperature, lignocellulosic content, and specific surface area was examined to investigate their impact on the properties of biochar. Finally, the potential biomedical applications of the biochar were assessed.

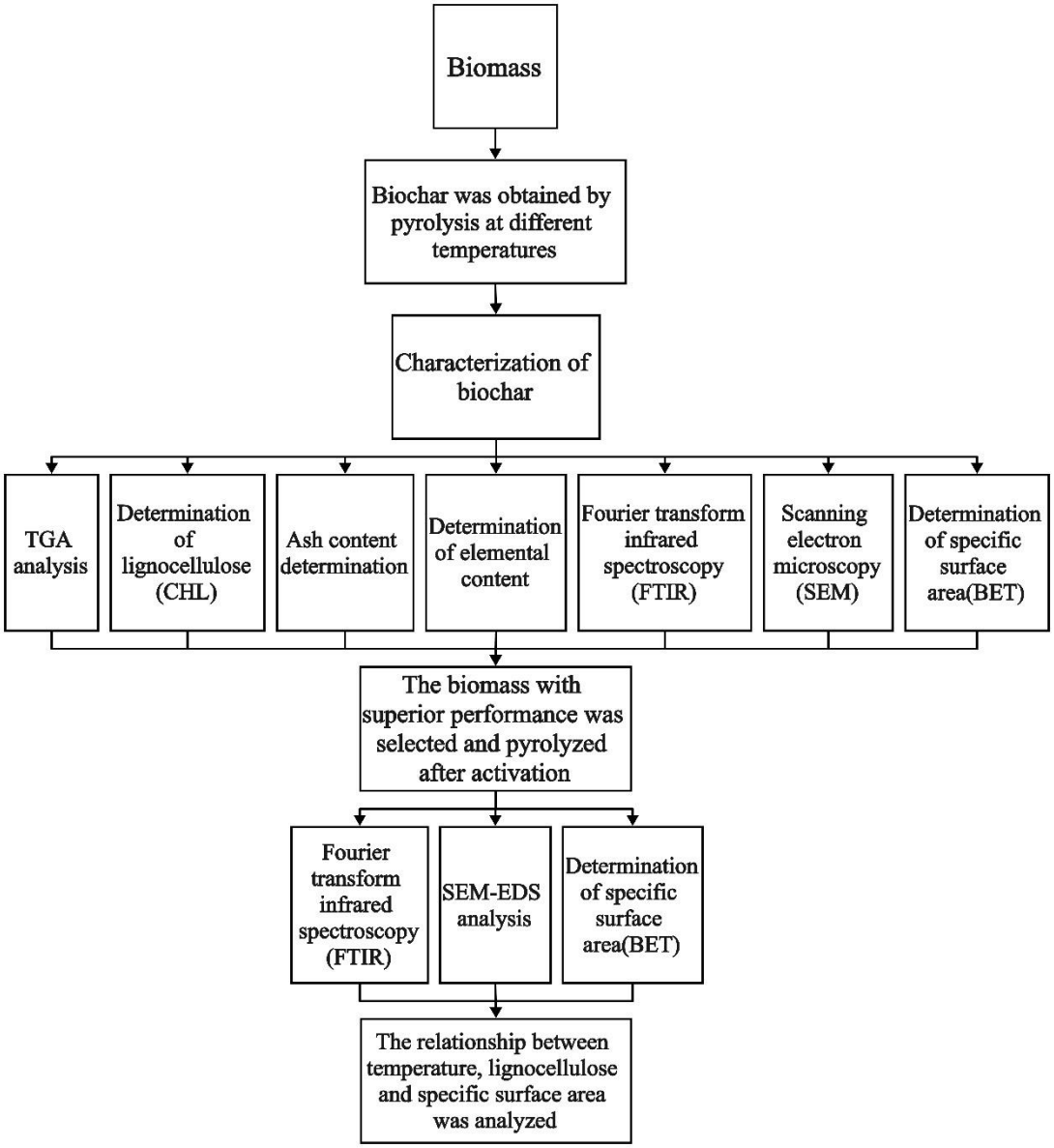

Figure 3.1 The research process of this experiment.

3.2.2 Pretreatment of biomass samples

The biomass undergoes pretreatment prior to pyrolysis: The collected biomass is dried in a vacuum drying oven (Model DZF-6050B) at 80℃ for 24 hours. This step effectively removes the moisture content from the biomass, enhancing subsequent processing efficiency. Additionally, it inhibits the growth of microorganisms and fungi,

thereby extending the storage duration. Following drying, the samples were ground using a multifunctional mill (Model 1000C), and the resulting biomass particles were sieved through a 65-mesh screen. The biomass pellets are transferred into sample bags and stored in glass containers containing drying powder.

3.2.3 Pyrolysis experiments of biomass and activated biomass

The pyrolysis experiments were conducted in a vertical tube furnace (OTF-1200X). Initially, the sample (10g) is weighed in a crucible and designated as W1. The sample is then placed in the centre of the glass tube to ensure uniform heating and subsequently inserted into the vertical tube furnace. After assembly, the lid is closed, and the pyrolysis process is initiated. The pyrolysis temperature procedure involves heating under N_2 (20mL min^{-1}) to 500, 600, 700, 800, and 900℃ at the rate of 10℃·min^{-1}. After holding for 60 minutes, the heating is terminated. The sample is then removed, cooled to room temperature, and weighed, with the result recorded as W2. The biochar yield is determined based on the mass difference between the initial and final samples. To ensure a uniform biochar sample for subsequent characterisation, the biocarbon sample is gently ground in the crucible for 5 minutes. The resulting biochar samples are denoted as CS500-CS900 (coconut shell biochar), PW500-PW900 (poplar wood biochar), BS500-BS900 (bamboo slice biochar), PS500-PS900 (peanut shell biochar), RS500-RS900 (rice straw biochar). All the biochar samples were then dried in the oven for 12 hours to obtain the final biochar sample. Finally, the crucible and glass tube, following pyrolysis, are placed into the muffle furnace (atmosphere box furnace, KJ-A1200-36L-IC) at 1000℃ for 90 minutes. The assembly is then allowed to cool to room temperature, facilitating the removal of residual biological oil and other substances for the next experiment. Figure 3.2 shows the pyrolysis flow chart.

The biochar yield is calculated according to the following formula:

$$Biochar\ yield = \frac{W_1}{W_2} \times 100\% \quad (5)$$

W_1(g) represents the dry mass of the biomass prior to hydrolysis, and W_2(g) represents the dry mass of post-pyrolysis biochar.

Figure 3.2 Image of pyrolysis equipment.

To prepare biological carbon with a large specific surface area, the biomass was activated and modified prior to nitrogen heat treatment. First, two 10g pieces of crushed poplar wood powder were each immersed in a 5M potassium hydroxide (KOH) solution at room temperature for 24 hours (soaking time). These samples were designated as K1 and K2. Then, the samples were placed in an oven and dried at 80℃ for 12 hours. The K1 mixture was then placed in the reactor and heated under a flow of N_2 (20mL min^{-1}) at a heating rate of 10℃·min^{-1} to 800℃ for 1 hour. After pyrolysis, the sample was washed with deionized water to achieve a neutral pH value and then dried in an oven at 80℃ for 12 hours. This sample was recorded as AKP. K2 was first washed with deionized water, then pyrolyzed and dried according to the above process. This sample was recorded as BKP. After drying, the two carbon samples were lightly ground for 5 minutes. The modified carbon was represented according to the type of pretreatment and the final temperature. For example, AKP800 represents the sample obtained through KOH activation treatment of the poplar wood at 800℃.

3.3 Characterisation of biochar

3.3.1 Thermogravimetric experiment (TGA)

This experiment utilized ASTM E1131-20 standard methods, which are commonly

employed in the industry to measure and predict the performance of specific fuels during combustion. The proximate analysis conducted in this study measured the weight percentages of moisture, volatile matter, ash, and fixed carbon in the biochar. The instrument selected was Synchronous DSC/TGA (SDT, Q600). The empty crucible was first weighed, and then approximately 10 mg of the sample was placed in the crucible. The instrument cover was allowed to close slowly, and the sample was heated at a rate of 10℃/min to 110℃ under a nitrogen (N_2) flow rate of 80 mL/min. The sample was then stored at 110℃ for 10 minutes to ensure complete water removal. The temperature was raised to 950℃ at a heating rate of 50℃/min. After 20 minutes of equilibrium, the nitrogen (N_2) flow was changed to oxygen (O_2) at a flow rate of 60 mL/min. The sample was maintained at 950℃ for an additional 30 minutes to ensure complete combustion. Finally, the sample was cooled to room temperature.

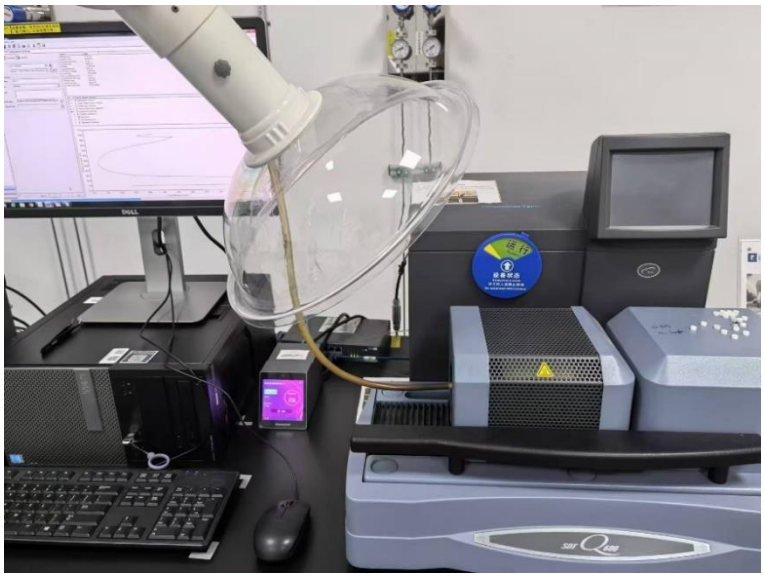

Figure 3.3 Image of the TGA instrument.

3.3.2 Determination of lignocellulose (CHL)

The lignocellulosic components of five types of raw biomass powder were analysed by gravimetric method[66]. The dried biological raw material (2 g) was weighed and placed into the Soxhlet extractor at a ratio of 2:1 with 490.5 mL of ethanol-acetone solution. The mixture was then boiled at 70°C for 4 hours. After extraction, the sample was dried overnight in a 105°C oven (blast dryer, DHG-9070A) using deionised water. The dried sample was marked as A and subsequently placed into 200 mL of 24%

potassium hydroxide (KOH) at 25°C for 4 hours. Following this, the sample was filtered, washed, and dried for 24 hours. The resulting sample was recorded as B. B was hydrolysed at room temperature for 3 hours using 200 mL of 72% sulfuric acid (H_2SO_4). Thereafter, the sample was filtered with 5% sulfuric acid (H_2SO_4) at 90°C for 2 hours of further reflux. The sample was dried at 80°C for 24 hours. The dry residue was weighed and recorded as C. The contents of cellulose, hemicellulose, and lignin in five biomass samples were calculated according to formulas (1) to (3).

$$\text{Cellulose } (\mathrm{B} - \mathrm{C}) \tag{6}$$

$$\text{Hemicellulose} = (\mathrm{A} - \mathrm{B}) \tag{7}$$

$$\text{Lignin} = \mathrm{C} \tag{8}$$

3.3.3 Ash content determination

To determine the ash content of biochar, 100 mg of dry sample was placed in a pre-weighed crucible. The sample was weighed with the crucible. Combustion of the sample was carried out in a muffle furnace at 950°C for 2 hours. Following cooling to room temperature, the crucible was removed, and its weight was subtracted to determine the ash weight. The ash percentage was derived using the following formula:

$$\text{Total ash} = \frac{W_a}{W_b} \times 100 \tag{9}$$

Where W_a (g) is the weight of the sample and W_b (g) is the weight of the ash.

3.3.4 Determination of elemental content

The content of C, H, N, and S elements in the biomass and biochar was determined using an elemental analyser. Using an Ultramicro electronic balance (MXS(SHEA)), 3 to 5 mg of biomass and biochar were carefully placed in tin foil and then transferred to the analyser for elemental determination. To ensure the accuracy of the experiment, each sample was determined three times.

3.3.5 Fourier transform infrared spectroscopy (FT-IR)

The FTIR profile of the dried biochar samples was determined using an infrared spectrometer (VERTEX 70). The measurement of diffuse infrared radiation reflection

was based on radiation absorption at specific frequencies, which allowed conclusions to be drawn about the functional groups on the biochar surface. The measurement was performed at room temperature. Prior to each measurement, the table surface was cleaned with deionised water, and the background was collected. Subsequently, within the OPUS program, the scanning wave number range was set to 500-4000 cm^{-1}, and the resolution was set to 4.0 cm^{-1}. The final map was obtained by accumulating 64 scans, followed by automatic baseline correction and smoothing. Spectral data for each sample were collected three times and averaged.

Figure 3.4 Image of the FTIR instrument.

3.3.6 Scanning electron microscopy (SEM)

SEM was employed to investigate the surface structure of biochar particles. Prior to the experiment, the biochar samples were dried overnight at 80°C. Subsequently, a 100 mg sample was taken using a spoon and spread on the carbon tape, followed by coating with a metal film to improve the electrical conductivity of the sample. The surface morphology of the biochar was observed by SE2 at 500× and 1000× magnification, respectively.

Figure 3.5 SEM equipment (left) and EDS instruments (right).

3.3.7 Determination of specific surface area (BET)

Biochar was analysed for specific surface area and porosity using the Brunauer-Emmet-Teller (BET) method. High-performance Dynamic Adsorption Analyser (3FLEX) was used to determine the nitrogen adsorption isotherm at -196°C (liquid nitrogen temperature). Figure 3.6 shows the degassing equipment and the BET experimental equipment. The sample preparation process and BET test method are as follows: the weighing air pipe + stopper is recorded as M1. The 0.07g dried sample is put into the tube, and the weight of the sample + tube + plug is recorded as M2. Subsequently, the sample was degassed at 300°C under a vacuum environment < 0.1 Pa for at least 12 hours to ensure the removal of physically adsorbed water and other gases. After degassing, the sample + tube + plug is denoted as M3. It is important to note that the degassing process is considered correct when $M2 \geq M3$ is confirmed. After completing the above steps, M1 and M3 were input into the software, and the BET template was selected to start the test. Using the multi-point BET method, N_2 adsorption data with a relative pressure range of 0.05 - 0.3 were used to calculate the specific surface area.

Figure 3.6 Image of the BET instrument.

4. RESULTS AND DISCUSSION

4.1 Introduction

The performance of biochar in various applications primarily depends on its properties, with surface area and porosity being among the most critical factors. These properties determine the quality of activated carbon within the biochar, thereby enhancing characteristics such as adsorption capacity. Broadly, larger pores aid in the diffusion of compounds, medium-sized pores serve as transfer channels, and smaller pores allow for molecular entrapment. Research on methods to produce biochar with a high pore structure and large surface area is a significant focus in this field.

This chapter examines the production of biochar with enhanced surface area and porosity by selecting different biomass feedstocks, optimising pyrolysis parameters (such as temperature), and applying modification treatments. The study explores the physical and chemical properties of biochar in relation to variations in production conditions, feedstocks, and activation agents. Biochar production process, raw materials, physical, chemical, and proximate and ultimate analysis are included in the experimental analysis. Additionally, the chapter discusses the influence of pyrolysis conditions and feedstocks on surface area, the effect of modified biochar on surface area enhancement, the evaluation of biochar's applicability in specific fields, and concludes with final observations.

4.2 Properties of biomass

4.2.1 Thermogravimetric analysis (TGA)

There are organic and inorganic components to biomass and it typically consists of approximately 90% organic matter (including water) and up to 10% inorganic ash. These components are concentrated differently according to the plant's biomass type, tissue, and growth stage[67]. A series of thermogravimetric analysis (TGA) experiments were conducted to analyse the chemical compositions of five different biomass materials: poplar wood (PW), bamboo slice (BS), coconut shell (CS), peanut

shell (PS), and rice straw (RS). The proximate analysis of the samples, as shown in Table 4.1, reveals distinct composition distributions among the different biomass materials. The water content of the five biomass types ranges from 2.44% to 6.37%. The higher water content in rice straw (6.37%) and bamboo slice (6.17%) suggests that these biomass types require more energy for dehydration during pyrolysis, potentially affecting pyrolysis efficiency and biochar yield. In contrast, poplar wood (2.57%) and coconut shell (2.44%) have lower water content, which could help reduce energy consumption during pyrolysis and improve the fixed carbon conversion rate.

The volatile content in the five types of biomass ranged from 70.19% to 80.14%. Peanut shell had the lowest volatile content at 70.19%, while poplar wood (80.14%) and coconut shell (78.37%) had the highest. In pyrolysis, heat facilitates a more thorough breakdown of biomass, which is attributed to the enhanced thermal decomposition of these two biomass types. As significant amounts of volatile components are removed, the carbon content in the residue becomes more concentrated, increasing the fixed carbon content. Higher fixed carbon content promotes the formation of porous structures with a large specific surface area in biochar. As the volatile components in biomass decompose and release gaseous products, such as water vapour, carbon dioxide, and methane, these gases create numerous pores within the biochar.

The fixed carbon content ranges from 13.25% to 19.17%. The fixed carbon content of peanut shell (19.17%) and coconut shell (18.37%) is high, indicating that these two kinds of biomass will leave a relatively stable and pure solid carbon phase after pyrolysis. This structure is not only conducive to improving the mechanical strength of biological carbon, but also can improve its chemical stability and durability in multiple uses, and can keep the pore structure from collapsing. Moreover, the solid carbon skeleton will undergo the process of rearrangement and graphitisation, and it is easier to form a highly ordered graphitic carbon layer when the highly fixed carbon is molten, and there are a large number of micropores between the ordered carbon layers. This

rearrangement greatly increases the specific surface area of biochar. Rice straw (13.25%), by contrast, had the lowest fixed carbon content.

The ash content of biomass varies significantly across different species. Poplar wood, bamboo slices, and coconut shells have ash contents of around 1%, while peanut shells (5.52%) and rice straw (6.20%) have slightly higher values. Although ash content is relatively low, it significantly influences pyrolysis behavior. Previous studies have reported that inorganic minerals in ash exhibit catalytic effects on biomass pyrolysis[68]. Experimental data also show a negative correlation between ash and carbon content (from elemental analysis), where higher ash content corresponds to lower carbon content, and vice versa. This relationship is due to the complementary nature of the organic and inorganic components in biomass. The carbon C atom forms the backbone of the organic structure, so C content represents the organic fraction, while ash content reflects the inorganic fraction, explaining their negative correlation[69]. Furthermore, the C atom contributes not only to C-containing molecules in biochar (identified as fixed carbon in proximate analysis) but also to small gaseous molecules in volatile substances (identified as volatile content in proximate analysis). Lastly, ash content is affected by temperature due to the complex interactions of thermal decomposition, volatilisation, mineral transformation, and selective retention of components. The outcome depends on the inorganic mineral composition of the biomass, such as the high silicon dioxide (SiO_2) content in rice straw, which may influence the purity and chemical properties of the resulting biochar.

Table 4.1 Proximate analysis of samples (%)

Sample	M	VM	FC	Ash
Poplar Wood	2.57	80.14	16.27	1.02
Bamboo Slice	6.17	77.64	15.25	0.94
Coconut Shell	2.44	78.37	18.37	0.83
Peanut Shell	5.11	70.19	19.17	5.52
Rice Straw	6.37	74.18	13.25	6.20

M: moisture, VM: volatile matter, FC: fixed carbon

4.2.2 Elemental analysis of biomass

The elemental analysis of biomass raw materials is presented in Table 4.2. Biomass is primarily composed of carbon (C) and oxygen (O), which together account for approximately 93%, followed by about 6% hydrogen (H) and less than 1% nitrogen (N) and sulphur (S). The oxygen content in rice straw is notably high, at 52.95%, but it has the lowest recorded carbon content, just over 40%. In contrast, poplar wood and coconut shells show the highest carbon contents, at 46.72% and 48.39%, respectively. Generally, woody biomass tends to have a higher carbon content compared to other types of biomass. The hydrogen content across these five biomass types is fairly consistent, ranging between 5% and 7%. It is also worth noting that sulphur is present in very small quantities across all biomass types, and is entirely absent in coconut shells.

Regarding ash composition, peanut shells and rice straw exhibited significantly higher ash content (5.52-6.20%), whereas poplar wood, bamboo slices, and coconut shells showed lower values (0.83-1.02%). Inorganic elements such as potassium (K), calcium (Ca), and silicon (Si) in ash play a crucial role in regulating the pyrolysis process. In low-ash materials such as poplar wood, bamboo slices, and coconut shells, the catalytic effect of K is predominant, reducing pyrolysis activation energy to promote cellulose cleavage and induce micropore development[70]. Although peanut shells are classified as a high-ash material, K and Ca act as co-catalysts during pyrolysis. However, a small amount of Si present in peanut shells was observed to weaken the catalytic activity of

K and Ca. Rice straw exhibits a high ash content and is predominantly composed of Si. Excess Si inhibits the exposure of active sites of K and Ca, reducing pyrolysis efficiency and jointly blocking biochar pore channels with molten ash[71].

Table 4.2 Ultimate analysis of biomass (%)

Sample	Ash	C	H	S	N	O
Poplar Wood	0.94	46.72	6.27	0.02	0.15	46.85
Bamboo Slice	1.02	44.68	6.08	0.02	0.24	48.99
Coconut Shell	0.83	48.39	6.12	0.00	0.12	45.37
Peanut Shell	5.52	45.97	6.15	0.05	0.74	47.09
Rice Straw	6.20	40.32	5.86	0.08	0.79	52.95

*The mass percentage of O element is estimated by difference subtraction, O%=100%-C%-H%-N%-S%-ash%, C-carbon, H-hydrogen, S-sulphur, N-nitrogen, and O-oxygen

4.2.3 Analysis of lignocellulose content

Biomass primarily consists of three organic components: cellulose, hemicellulose, and lignin, collectively referred to as lignocellulose. The amount, proportion, and type of each component in lignocellulose depend largely on the raw material[72]. The lignocellulosic composition of the tested biomass samples is presented in Table 4.3. Cellulose was the most abundant component in all tested biomass (except rice straw), followed by lignin and hemicellulose. The polysaccharides in cellulose and hemicellulose are crucial for biomass energy conversion, and their content determines fuel conversion efficiency[73]. The cellulose content in poplar wood and coconut shells reached 51.36% and 51%, respectively. During pyrolysis, cellulose contributes to the synthesis of volatile products, meaning that high cellulose content can result in a high volatile content, as shown in the proximate analysis of poplar wood (80.14%) and coconut shell (78.37%). Additionally, the pyrolysis of cellulose releases water vapor, carbon dioxide, carbon monoxide, methane, light organic compounds, tar, and other products. The release of gases and liquids facilitates pore formation, increasing the specific surface area. The high mass loss rate of cellulose alters the porous structure and specific surface area of pyrolytic biochar, which also supports the formation of

graphite biochar[74].

The decomposition mechanism of lignin is highly complex due to its amorphous, three-dimensional network structure composed of carbon-oxygen and carbon-carbon bonds[75]. Lignin crosslinks with cellulose and hemicellulose, and its complex chemical structure makes decomposition more challenging. Additionally, lignin serves as the primary precursor for biochar formation during biomass pyrolysis and possesses a highly aromatic structure, contributing to increased biochar yield. For instance, peanut shells contain 31.47% lignin and exhibit the highest biochar yield among the five biomass types, ranging from 28.40% to 33.96%. Coconut shells, with 25.15% lignin, have a biochar yield between 26.64% and 30.53%. Rice straw, with the lowest lignin content of 17.13%, produces biochar yields of 28.47% to 33.41%, likely due to its high ash content. The inorganic minerals in the ash exhibit high thermal stability and remain in the carbonised residues.

To produce biochar with enhanced physicochemical properties, such as high fixed carbon content (FC), large specific surface area (S_{BET}), and a high-quality aromatic structure, selecting biomass with high cellulose and lignin content is advantageous for thermochemical transformation processes like pyrolysis. The choice of specific biomass feedstocks significantly influences the total biochar yield, its physicochemical properties, and the overall economic viability and conversion efficiency of the pyrolysis process.

Table 4.3 Content of lignocellulose in different biomass (%)

Biomass	Cellulose	Hemicellulose	Lignin
Poplar Wood	51.36	17.00	22.10
Bamboo Slice	46.54	27.26	19.36
Coconut Shell	51.00	16.28	25.15
Peanut Shell	45.22	13.17	31.47
Rice Straw	41.83	23.23	17.13

4.3 Properties of biochar

4.3.1 Biochar yield

The bio-carbon yields from poplar wood, bamboo slices, coconut shells, peanut shells, and rice straw, as shown in Fig. 4.1, decrease progressively with increasing pyrolysis temperatures, with the most notable decline occurring between 500℃ and 700℃. In contrast, the trend becomes more gradual within the pyrolysis temperature range of 700°C to 900°C. When the pyrolysis temperature is less than 800℃, the biocarbon yield of peanut shells is slightly higher than that of rice straw, but at 900℃, the biochar yield order of these two kinds of biomass changes. In the whole pyrolysis range, the biocarbon yield of peanut shell and rice straw is relatively close, the biocarbon yield of coconut shell is relatively close to that of bamboo slice, and it is in the middle position, while the biochar yield of poplar wood is the lowest. Overall, the order of biochar yield from low to high was as follows: poplar wood biochar < bamboo slice biochar < coconut shell biochar < rice straw biochar < peanut shell biochar. The difference in biochar yield indicates that the composition of bio-carbon changes with the change of pyrolysis temperature and biomass raw material.

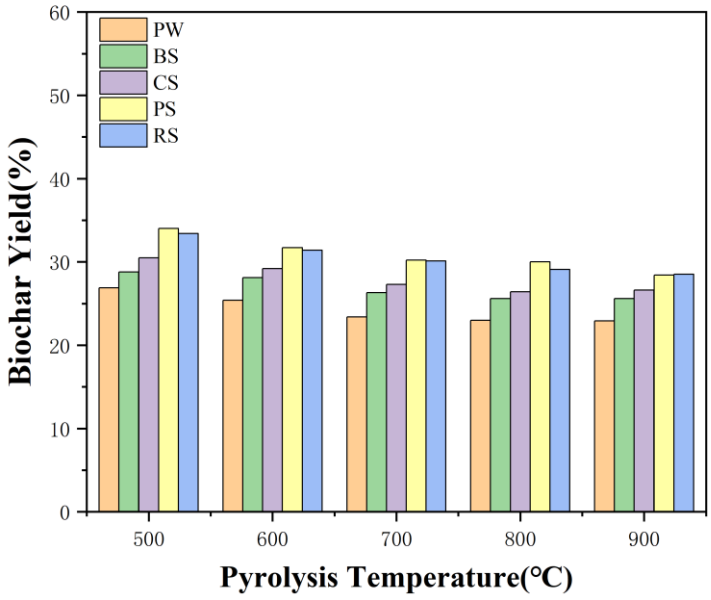

Figure 4.1 The yield of biochar prepared at different pyrolysis temperature.

4.3.2 Ash content of biochar

Biochar ash refers to the solid residue remaining after the biochar is burned at high temperatures in the presence of air. It is primarily composed of inorganic minerals, such as those containing potassium, silicon, calcium, aluminium, and iron. Figure 4.2 shows how the ash content of biochar changes with pyrolysis temperature. As temperature increases, the ash content of biochar from poplar wood, bamboo slices, coconut shells, peanut shells, and rice straw also increases, indicating that the inorganic content of biomass-derived biochar rises with a higher degree of carbonisation. At the same pyrolysis temperature, the ash content of poplar wood, coconut shells, peanut shells, and bamboo slices is similar, all below 10%, while the ash content of rice straw (24.5%-27.9%) is significantly higher. This indicates that rice straw contains less organic matter compared to other types of biomass. As a result, rice straw releases fewer volatile compounds during the pyrolysis process, leading to a less developed pore structure. Additionally, the ash produced tends to block the micropores, further reducing the surface area of the biochar.

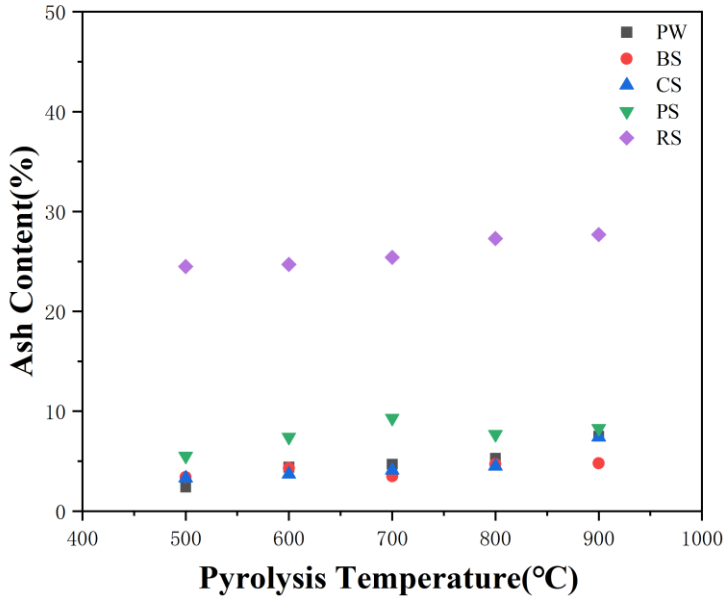

Figure 4.2 Ash content of biological carbon prepared at different pyrolysis temperatures.

4.3.3 Elemental analysis of biochar

Table 4.4 lists the contents of C, H, N, S, and O in biochar, and Figure 4.3 illustrates the trends of these elements in the organic components of biochar at pyrolysis temperatures of 500, 600, 700, 800, and 900°C (with oxygen content calculated by subtraction). The possible medical applications of biochar were assessed based on various properties, such as atomic ratios of (N+O)/C and H/C. Carbon content in biochar increases significantly as pyrolysis temperature rises, as shown in figure 4.3 (a). In PW500-PW900, this increase is notable, with carbon content rising from 74.50% to 90.01%. This is largely due to the high lignin content in coconut shells, and as the temperature increases, non-carbon components such as volatile organic compounds and water break down and escape, resulting in a higher concentration of fixed carbon in the remaining solid material.

However, the carbon content of RS500-RS900 is only between 52.72% and 55.83%, indicating low carbonisation efficiency. This may be related to the unique chemical composition of rice straw, which contains different proportions of cellulose, hemicellulose, and lignin compared to other biomass, and a higher proportion of inorganic salts, especially silicates. These inorganic components do not evaporate during pyrolysis but instead form solid residues, diluting the carbon content. Furthermore, the high ash content may hinder effective carbonisation, resulting in biochar that is a mixture of ash and incompletely carbonised organic matter. As elemental carbon is the key component of biochar, enhancing its quality increases its potential for value-added applications.

Additionally, the H and O elements exhibited a gradual decrease with increasing temperature (Figure 4.3 (a, b)). The pyrolysis of poplar wood, bamboo slices, coconut shells, peanut shells, and rice straw involves carbon enrichment and the removal of oxygen from organic components. At higher temperatures, weaker bonds break down further, resulting in higher yields of gaseous products. For example, dehydrogenation leads to the formation of H_2, cleavage of hydroxyl (-OH) structures releases H_2O[76],

and the carboxyl group (-COOH) may release CO_2 or CO. The oxygen content in coconut shell samples (CS700-CS900) sharply decreased from 7.85% to 0.23%, indicating that more intense pyrolysis reactions occur in coconut shells above 700℃. The decomposition of a significant number of oxygen-containing functional groups into CO_2, CO, and H_2O, coupled with the reorganisation of the internal carbon structure and enhanced carbonisation, results in a substantial reduction in oxygen content.

Ash content is generally increasing, but the rate of growth trend is different. The ash content of poplar wood and coconut shell increased significantly from 2.35%, and 3.34% to 7.54% and 7.43% respectively. The growth of the other three species was relatively gentle, and the ash content of bamboo slice biochar fluctuated. However, the ash content of rice straw biochar was the highest and much higher than that of the other four biochar, and the range was even as high as 24.46% to 27.69%. This may result in a looser structure of biochar, with significant negative effects on porosity, specific surface area, and adsorption capacity.

The nitrogen content of the five biochar varies with temperature. All biochar contains less than 1% nitrogen, except for PS500 and RS500. This finding is reassuring from a safety perspective and is likely due to the removal of nitrogen or other nitrogen-containing volatile compounds, such as ammonia, at high temperatures[77]. Regarding sulphur content, only RS500 through RS900 exhibit sulphur levels ranging from 0.11% to 0.26%, while all other biochar has sulphur content below 0.1%. Notably, no sulphur was detected in PW500 through PW900, which is advantageous as excessive sulphur can lead to toxicity or reduced biocompatibility in organisms.

Table 4.4 Ultimate analysis biochar (%) and atomic ratio [H/C, O/C, (N+O)/C]

Sample	Ash	C	H	S	N	O	H/C	O/C	(N+O)/C
PW500	2.35	73.56	3.23	0.00	0.27	20.59	0.52	0.21	0.21
PW600	4.36	74.31	2.60	0.00	0.27	18.47	0.42	0.19	0.19
PW700	4.72	79.22	1.90	0.00	0.21	13.95	0.29	0.13	0.13
PW800	5.32	80.22	1.69	0.00	0.28	12.50	0.25	0.12	0.12
PW900	7.54	80.57	1.50	0.00	0.30	10.10	0.22	0.09	0.10
BS500	3.41	76.61	3.23	0.00	0.43	16.32	0.50	0.16	0.16
BS600	4.29	77.65	2.63	0.00	0.40	15.03	0.40	0.15	0.15
BS700	3.46	79.79	2.05	0.01	0.42	14.27	0.31	0.13	0.14
BS800	4.72	82.02	1.89	0.05	0.48	10.83	0.27	0.10	0.10
BS900	4.78	84.69	1.53	0.06	0.51	8.44	0.22	0.07	0.08
CS500	3.34	74.50	2.63	0.02	0.18	19.33	0.42	0.19	0.20
CS600	3.73	76.11	2.89	0.02	0.20	17.06	0.45	0.17	0.17
CS700	4.12	85.84	1.95	0.07	0.18	7.85	0.27	0.07	0.07
CS800	4.46	88.97	2.63	0.04	0.24	3.67	0.35	0.03	0.03
CS900	7.43	90.01	1.96	0.02	0.36	0.23	0.26	0.00	0.01
PS500	5.50	68.82	3.09	0.04	1.02	21.53	0.53	0.23	0.25
PS600	7.37	68.36	2.37	0.04	0.95	20.91	0.41	0.23	0.24
PS700	9.30	72.00	1.84	0.06	0.67	16.13	0.30	0.17	0.18
PS800	7.73	73.82	1.59	0.05	0.69	16.09	0.26	0.16	0.17
PS900	8.25	74.58	1.48	0.09	0.57	15.02	0.24	0.15	0.16
RS500	24.46	52.72	2.74	0.13	1.17	18.78	0.62	0.27	0.29
RS600	24.65	54.39	2.17	0.26	0.93	17.60	0.47	0.24	0.26
RS700	25.44	54.99	1.70	0.14	0.88	16.85	0.37	0.23	0.24
RS800	27.34	55.57	1.59	0.11	0.93	14.46	0.35	0.20	0.21
RS900	27.69	55.83	1.52	0.11	0.90	13.95	0.32	0.19	0.20

*The mass of O element is estimated by difference subtraction, O%=100%-C%-H%-N%-S%-ash%, C-carbon, H-hydrogen, S-sulphur, N-nitrogen, and O-oxygen

Cellulose and hemicellulose in biomass are rich in hydrogen (H) elements, such as methylene (-CH_2), while polar functional groups, including hydroxyl (-OH) and amino (-NH_2), contain oxygen (O) and nitrogen (N) elements. while the atomic ratios of H/C and O/C (or (N+O)/C) can reflect the characteristics of biochar. The H/C ratio indicates the transformation of biochar's carbon structure from hydrocarbons to aromatic rings, which can be used to assess its aromaticity[78]. As can be seen from Fig 4.3 (c), with the increase in pyrolysis temperature, the H/C atomic ratio decreases significantly, indicating that the depolymerisation process is taking place, which means that the oxidation resistance increases[79]. According to the International Biochar Initiative (IBI), there are two critical points for the H/C atomic ratio, one at 0.4 and the other at 0.7. A ratio below 0.4 indicates highly stable carbon, while 0.4-0.7 indicates stable carbon. The results show that, at 700℃-900℃, the H/C ratio of each biochar is below 0.4, indicating a highly stable carbon structure with a well-developed aromatic ring configuration[80]. It has high stability and resistance.

The O/C ratio is used to assess the oxidation level of biochar. O/C (or (N+O)/C) can also indicate the degree of polarity of biochar with polar functional groups, reflecting the hydrophobicity of biochar. Biochar tends to accumulate aliphatic and aromatic compounds within its pores and on its surface, but these compounds are reduced as the temperature increases[77]. Due to decarboxylation, the O/C ratio decreases, suggesting that biochar becomes highly carbonised, forming a stable carbon structure. The results show (Fig 4.3 (d)) that the O/C and (N+O)/C of all biochar gradually decrease as the temperature increases from 500℃ to 900℃. Indicates a decrease in polarity, potentially due to increased hydrophobicity and a lower number of polar functional groups on the surface[81]. In addition, there are also differences in polarity. At the same pyrolysis temperature, the biochar from poplar wood and coconut shells, which exhibit a higher degree of carbonisation, differ in polarity, with poplar wood > coconut shells. It has been demonstrated that the increased polarity of poplar wood biochar offers more

adsorption sites, enhancing the adsorption process. Variations in aromaticity and polarity of biochar, depending on pyrolysis temperatures and different biomass feedstocks, can lead to differing adsorption characteristics.

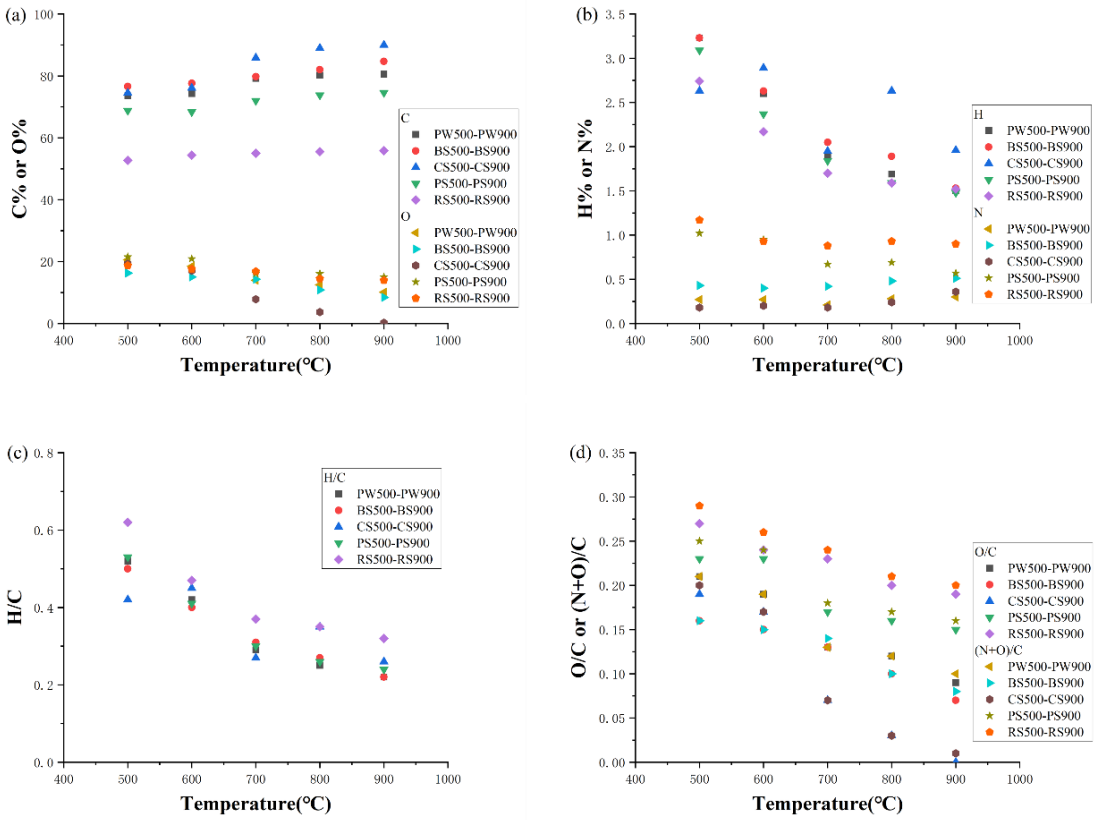

Figure 4.3 Elemental composition of organic components of different biochar at different temperatures.

4.3.4 Fourier transform infrared spectrum of biochar (FT-IR)

Thermal pyrolysis of biochar particles produced functional groups that were analysed by FTIR infrared spectroscopy. Figure 4.4 shows the infrared spectrum of poplar wood biochar. Broad absorption bands in the 3650-3200cm^{-1} range and 2900 cm^{-1} correspond to O-H stretch absorption and C-H stretch absorption. The absorptions can be attributed to the presence of hydroxyl groups and abundant carbon-hydrogen bonds within the main biomass constituents: cellulose, hemicellulose, and lignin. The gradual reduction of these two peaks indicates partial degradation of the polysaccharide structure, and the residual cellulose persists for a longer reaction time. The peaks at 2500-2100cm^{-1} are

attributed to the absorption peak of CO_2, and the CO_2 concentration remains constant as the temperature increases. In general, the formation of carbon-oxygen compounds is associated with clusters of two types of ether bonds[82]. At low temperatures, ether Bridges (such as ether bonds connecting lignin subunits) in lignin are the main source of carbon oxides. At higher temperatures, diaryl ether dissociates, while the secondary cracking of volatiles mainly produces CO_2[83]. The absorption peaks at 1890cm^{-1} are asymmetric stretching of glucuronic acid carboxyl groups in hemicellulose and C=O stretching bands of lignin-conjugated carbon groups[84]. For PW500-PW800, C=O is enhanced at 1890 cm^{-1}. When the temperature rises to 900°C, the absorption of C=O gradually weakens, indicating that the carbon-based is decomposed or transformed into other forms at high temperatures. The stretching vibrations of the C=C double bond in lignin at 1590cm^{-1} are usually associated with aromatic compounds. With the increase in temperature, the absorption peak of C=C is relatively stable, indicating that the directional structure is formed and retained at high temperatures. In addition, 1400cm^{-1} is assigned to C-H bands in the plane deformation of aromatic ring stretching in lignin[85]. And 850-750 cm^{-1}, 1100 cm^{-1} of the absorption peaks corresponding cellulose and hemicellulose in β-(1-4)- glycosidic bond of C-O-C stretching and aromatic hydrocarbon key bending tensile[84]. For PW900, the polar functional group (C-O-C) is significantly reduced, and this change also confirmed the change in the O/C ratio in the elemental analysis (Table 4.4). In summary, with increasing pyrolysis temperature, the biological carbon of poplar showed obvious dehydration, decarboxylation and aromatisation, and its polarity decreased, and a more stable aromatic carbon skeleton was formed.

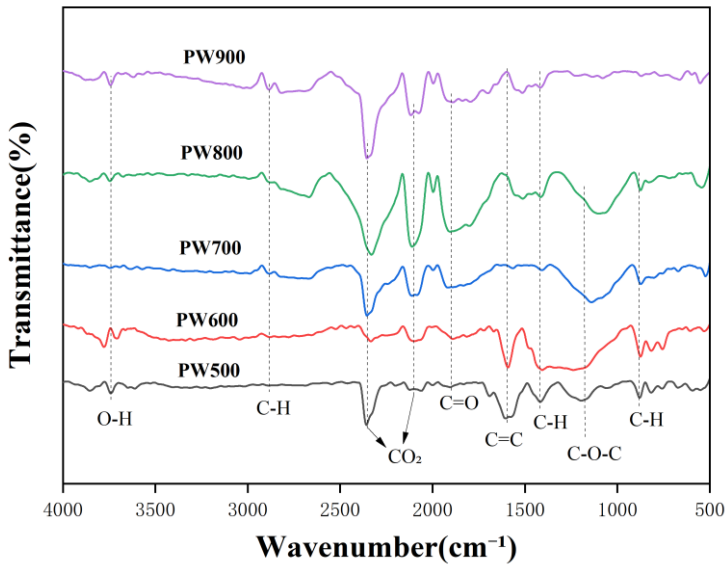

Figure 4.4 Fourier transform infrared spectrum of PW500-PW900.

Similar to poplar wood biochar, the organic carbon components of coconut shell biochar, bamboo slice flake biochar, peanut shell biochar, and rice straw biochar also changed (Fig 4.5, fig 4.6, fig 4.8). With increasing pyrolysis temperature, the C-H bonds and oxygen-based functional groups (C=O, phenol O-H, C-O-C) in cellulose and lignin gradually decline, while the aromatic C=C bonds are preserved. Particularly obvious is the coconut shell biochar, where the peak value of corresponding functional groups decreases significantly at PW800-PW900. This decrease is due to the breaking of the ether bond, especially at higher temperatures. The rapid volatilisation of oxygen and hydrogen can also correspond to the rapid reduction of their O/C ratio from elemental analysis.

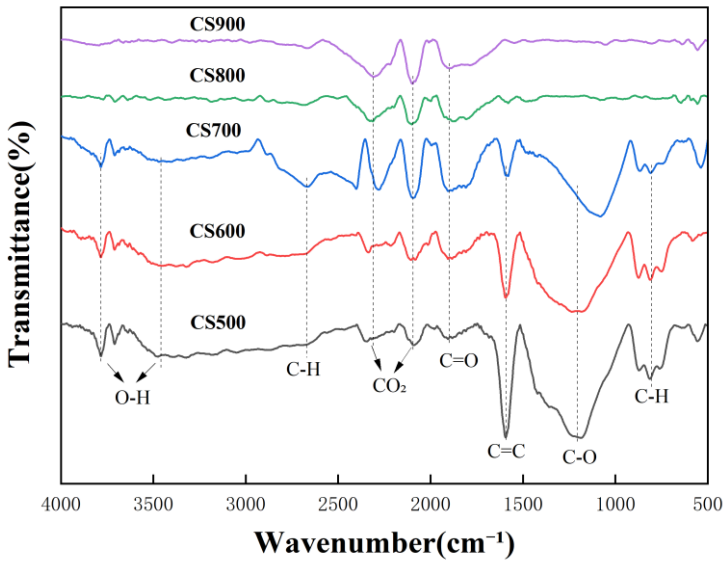

Figure 4.5 Fourier transform infrared spectra of CS500-CS900.

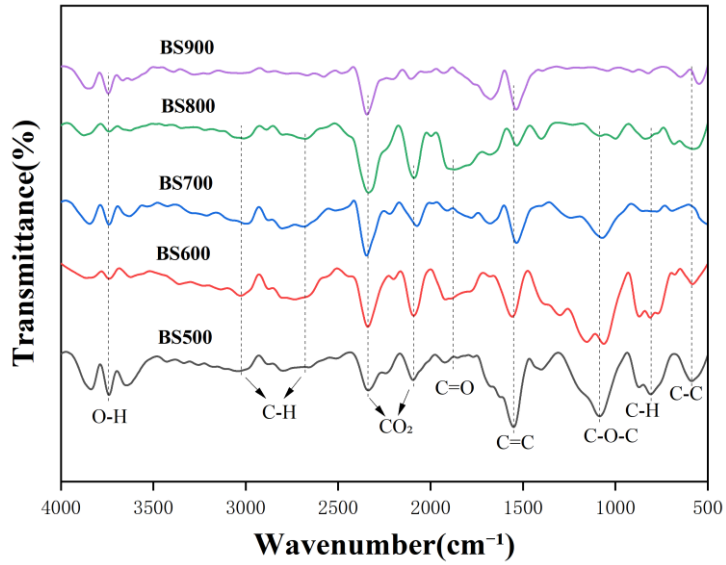

Figure 4.6 Fourier transform infrared spectra of BS500-BS900.

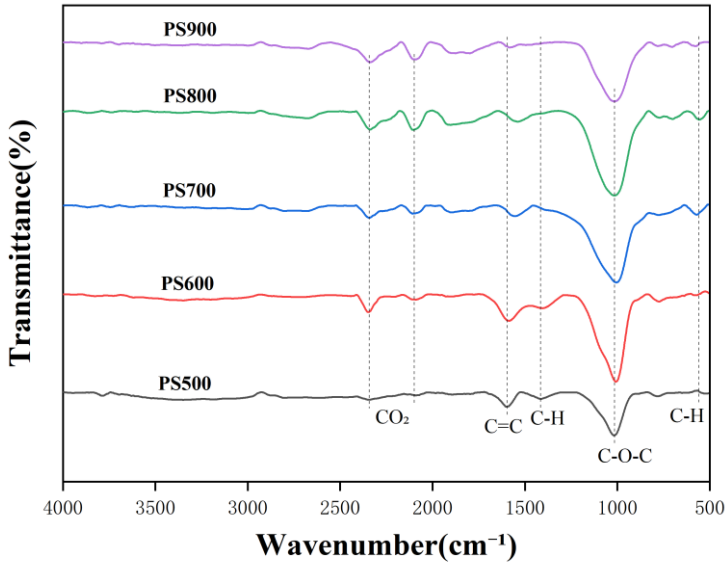

Figure 4.7 Fourier transform infrared spectra of PS500-PS900.

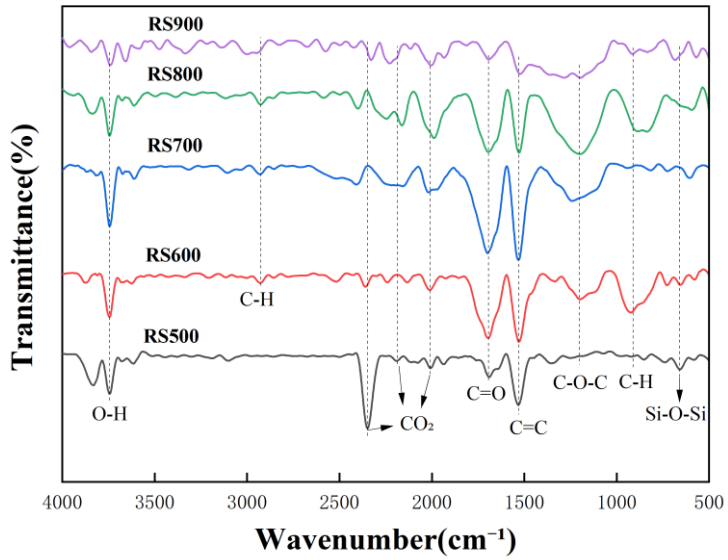

Figure 4.8 Fourier transform infrared spectra of RS500-RS900.

The difference is that obvious C-O-C absorption peaks (1200cm^{-1} and 1010cm^{-1}) can still be observed in RS900 and PS900 prepared at 900℃, while the absorption peaks of C-O-C (1084cm^{-1}) on BS900 are weak. In addition, the oxygen-containing functional group C=O of rice straw biochar (1530cm^{-1}), bamboo slice biochar (1875cm^{-1}), and coconut shell biochar (1900cm^{-1}) all decreased gradually, but no trace of C=O absorption peak was directly captured in PS500-PS900. At the same time, no traces of

hydroxyl (C-H) were detected, which may indicate that the peanut shell biochar itself contains less functional group content (Fig 4.7). Finally, due to the high content of SiO_2 in rice straw, significant vibration absorption from Si-O-Si was also observed at 665cm^{-1} of rice straw biochar[86]. The vibration absorption of Si-O-Si increased when the organic carbon disappeared gradually with the pyrolysis temperature, indicating that the high ash content of rice straw biochar was mainly derived from Si-containing minerals and their enrichment during pyrolysis.

4.3.5 Scanning electron microscopy of biochar (SEM)

The surface structure and pore development of biochar are closely interconnected, largely due to its diverse biomass sources, which exhibit varying morphological structures. Figures 4.9 to 4.13 show the surface morphology of biochar captured using scanning electron microscopy at magnifications of ×500 and ×1000. The shape of biochar can be categorised as fibrous, prismatic, or spherical[87]. The biochar derived from poplar wood displays distinct longitudinal fibre characteristics, likely originating from lignin, providing additional support and stability. At 500°C, the biochar particles appear compact and irregular, with few pores. The pore volume of PW700 and PW800 significantly increases with temperature, indicating that a substantial release of volatile matter during the carbonisation process leads to notable morphological changes. The sharp increase in pore quantity and their uniform distribution suggests a considerable expansion of the biochar surface area. Coconut shell biochar follows a comparable trend: CS500 biochar displays a hard, uneven surface with few pores. As the temperature rises to 600°C and 700°C, numerous pores emerge, and the surface becomes rougher. Additionally, the formation of many micropores significantly enhances the specific surface area. At temperatures between 800°C and 900°C, excessive heat causes structural breakdown, resulting in the disintegration of biochar and its dispersion across the surface. This is consistent with the subsequent surface area analysis, shows a sharp decrease in the surface area of coconut shell biochar at 800℃, likely due to the structural destruction.

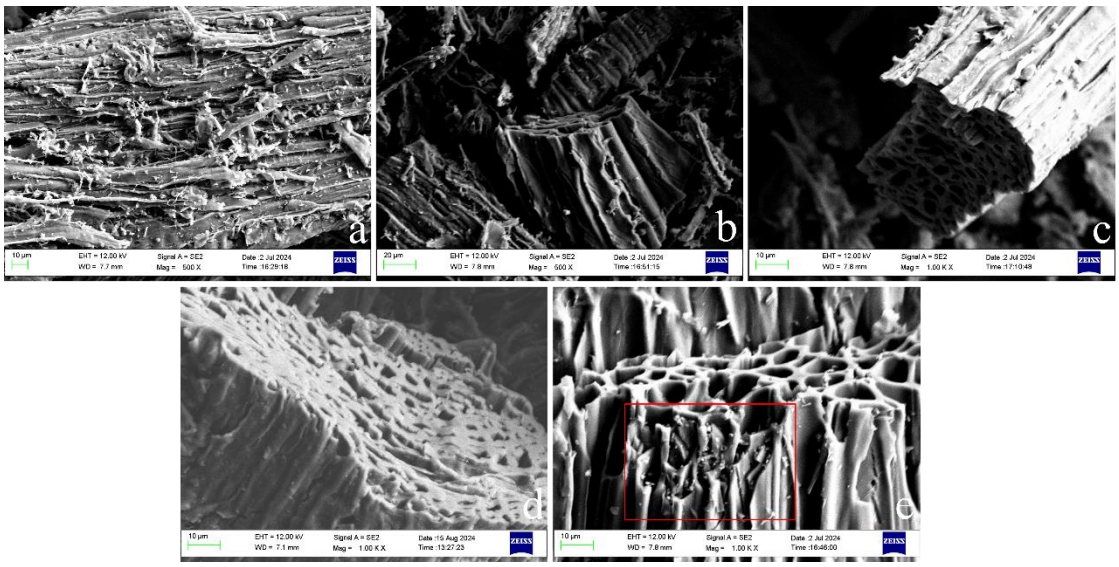

Figure 4.9 SEM images of (a) PW500, (b)PW600, (c)PW700, (d)PW800, (e)PW900.

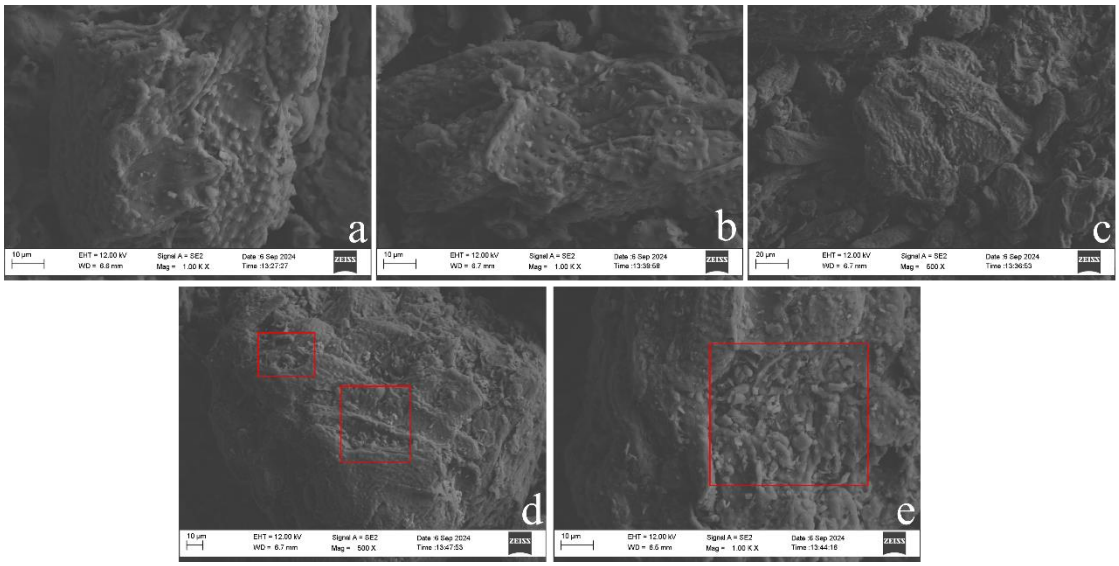

Figure 4.10 SEM images of (a) CS500, (b)CS600, (c)CS700, (d)CS800, (e)CS900.

The SEM images shown in Figure 4.11 show that the bamboo slice retained their fibre bundle shape after carbonisation, displaying parallel microstructures. The surface pore structures of BS600 and BS700 are marked by the presence of multi-layered pores, which arise from the voids created by biomass thermal decomposition and the escape of volatiles in the pyrolysis process[88]. The pore structure can be seen to collapse after the pyrolysis temperature is raised to up to 800°C, and blockage is clearly observed in BS900 in particular, which can lead to a decrease in surface area. An increase in pore size and micropores is observed in PS600, followed by significant fragmentation. High temperatures are likely to cause stronger cleavage reactions at 700°C and 900°C,

resulting in broken pore structures.

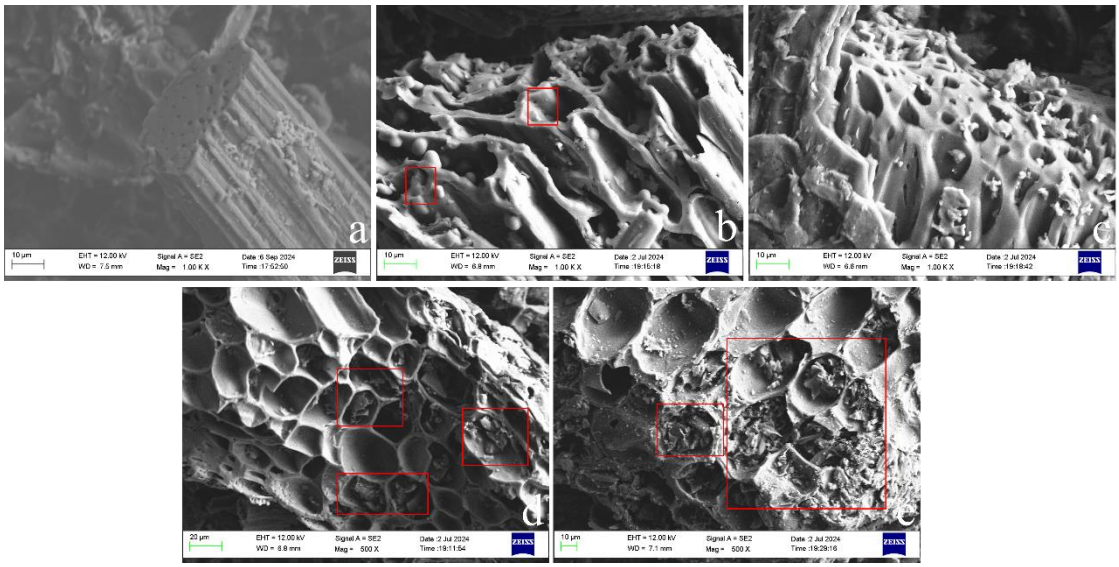

Figure 4.11 SEM images of (a) BS500, (b)BS600, (c)BS700, (d)BS800, (e)BS900.

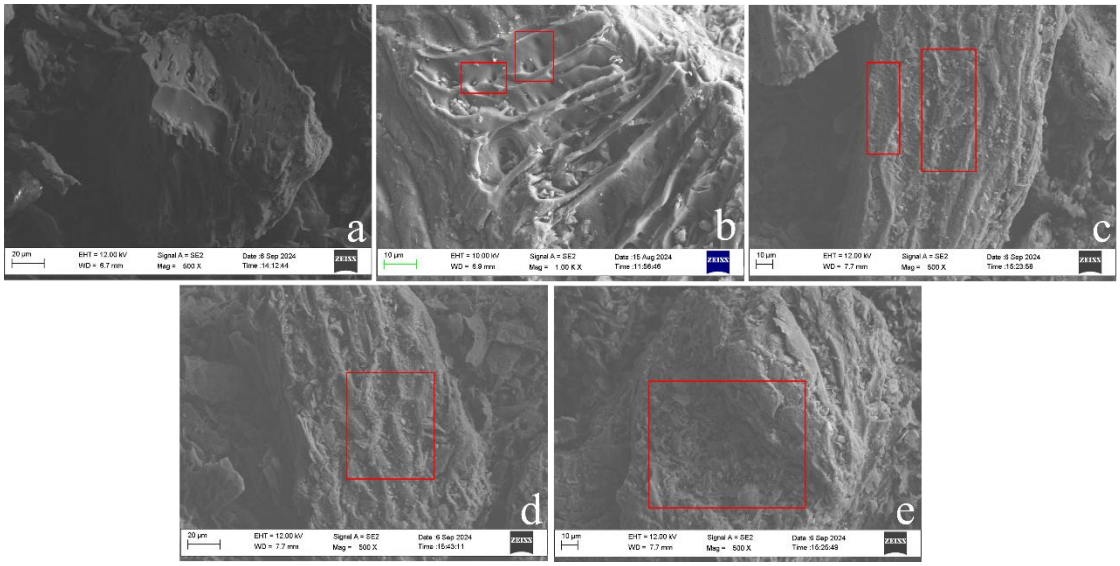

Figure 4.12 SEM images of (a) PS500, (b)PS600, (c)PS700, (d)PS800, (e)PS900.

As shown in Figure 4.13, rice straw biochar exhibits a slender, rod-like structure, and the development of micropores on the surface of RS500-RS900 is minimal. Although pore size increases with temperature, numerous particles accumulate on the carbon surface, forming dense aggregates[89]. This is likely due to the high ash content, such as silica and other components, which remain at elevated temperatures for longer periods, resulting in a suboptimal specific surface area for rice straw biochar. The primary characteristics and morphology of biochar depend on key factors such as pyrolysis temperature, biomass feedstock composition, and ash content. A range of

physical properties is observed in biochar samples following pyrolysis at various temperatures, depending on the composition of biomass feedstocks and the level of ash in the samples.

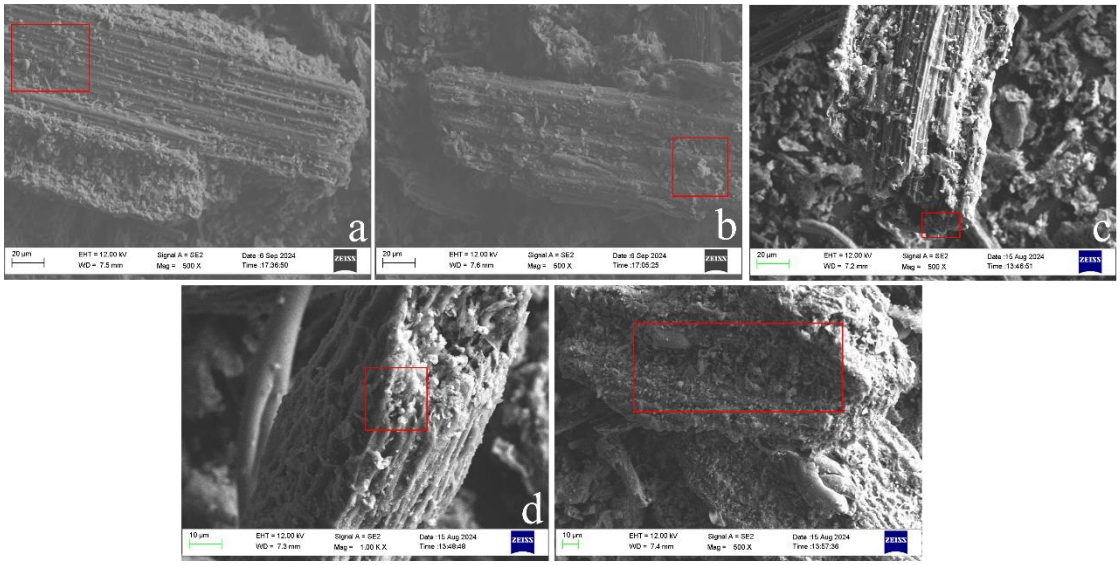

Figure 4.13 SEM images of (a) RS500, (b)RS600, (c)RS700, (d)RS800, (e)RS900.

4.3.6 Specific surface area analysis of biochar (BET)

Biochar typically exhibits a well-developed pore structure with a broad range of pore sizes. A high-temperature biomass pyrolysis activity produces nanopores, which have a significant adsorption capacity for small molecular organic pollutants (such as polycyclic aromatic hydrocarbons and nitrobenzene compounds). In order to determine the specific surface area of biochar, the Brunauer-Emmett-Teller (BET) method is recommended by the two most prominent global organisations: the European Biochar Certificate (EBC)[90] and the International Biochar Initiative (IBI)[91]. The specific surface area, micropore surface area, micropore volume, and total pore volume of the biochar samples are detailed in Table 4.5. As pyrolysis temperature rises, the specific surface area initially grows and subsequently diminishes. For PW500-PW800, a positive correlation between the specific surface area and pyrolysis temperature is observed. At 500°C, the specific surface area of PW500 is 116.36 m^2/g, significantly higher than that of the other four biochar at the same temperature. As the pyrolysis temperature increases from 500°C to 800°C, more thermal original amorphous biochar is produced. The increased carbonisation intensity enlarges the pore space or creates

additional pores, resulting in the continuous expansion of the specific surface area. The surface area suddenly jumps to 426.18 m^2/g at 700°C. This trend aligns with previous literature reports, yet the values obtained in this study exceed those reported in previous studies[92]. The pore volume and specific surface area are maximum at 800°C (451.06 m^2/g and 0.1458 cm^3/g, respectively). While surface area increases between PW700 and PW800, there is a minimal increase in pore structure at low pyrolysis temperatures. Additionally, by 700°C, most volatile compounds may have already been released, leading to a slower release rate and, consequently, a smaller increase in the specific surface area. Notably, at 900°C, the specific surface area decreases to 327.08 m^2/g. This reduction can be attributed to secondary polymerisation reactions, where excessive pore widening damages the micropores. Furthermore, the char structure begins to rearrange into a more ordered graphitic form, causing micropores to close or compress, thus reducing the surface area.

For coconut shell biochar, there was a significant increase in surface area from CS500 to CS600, exhibiting the optimal surface area of 464.66 m^2/g. As the temperature rose to 700℃, the surface area slightly decreased to 448.5 m^2/g. The variation in surface area and micropore volume, which was dependent on pyrolysis temperature, not only aligned with established literature trends but also demonstrated values higher than those reported previously[93]. These findings confirm the superior structural characteristics of this biochar. Interestingly, CS600 showed a slightly greater surface area than CS700, but the micropore area and volume were noticeably lower than CS700. This indicates that the pores of CS600 may have complex geometric shapes, while the surface area of CS700 is mainly contributed by micropores. The high micropore area of CS700 makes it highly suitable for adsorbents as it can provide more reaction activity and selectivity. For example, in drug delivery systems, a high micropore volume can effectively store and slowly release drugs, making CS700 more promising for practical applications. A significant reduction in specific surface area to 32.2 m^2/g was observed as pyrolysis temperature increased. This phenomenon is attributed to pore widening, coalescence of

adjacent pores, and material melting, softening, and fusion processes, consistent with previous studies[94].

In contrast, the maximum surface area of bamboo slice biochar and peanut shell biochar is much less, showing the best surface area at 700℃ (252.18 m^2/g) and 600℃ (319.02 m^2/g), respectively. These findings are consistent with previously published research[95]. The specific surface area of bamboo slice biochar is more obvious than that of peanut shell biochar, which may have a great relationship with their raw materials and chemical composition. The pyrolysis temperature of bamboo slice and peanut shell biochar decreased to 56.2 m^2/g and 79 m^2/g at 900℃, respectively. This indicates that secondary reactions such as thermal cracking, devolatilisation, aromatisation, decarboxylation and dehydration lead to surface disintegration and fragmentation of biochar, which can be clearly seen in Figure 4.11. It is worth mentioning that the surface area of RS500 - RS900 is generally low, with a maximum of 45.98 m^2/g, which is similar to previous studies[96]. This result shows that the RS series pores are not obvious, which may mean that the pores within the biochar are a dead end[97]. Moreover, biochar contains more ash content (24.46% to 27.69%), which reduces the surface area by filling or blocking the contact of micropores.

Table 4.5 Pore parameters of biochar

Samples	Specific Surface Area	Micropore Surface Area	Micropore Volume Pore	Total Volume Pore
	S_{BET} (m^2/g)	S_{mic} (m^2/g)	V_{mic} (cm^3/g)	V_{total} (cm^3/g)
PW500	166.36	91.08	0.0369	0.0581
PW600	348.37	235.10	0.0929	0.1105
PW700	426.18	311.91	0.1210	0.1364
PW800	451.06	336.01	0.1302	0.1458
PW900	327.08	226.49	0.0897	0.1026
BS500	37.08	24.17	0.0097	0.0126
BS600	116.15	68.57	0.0280	0.0324
BS700	252.18	161.74	0.0643	0.0823
BS800	90.08	88.13	0.0327	0.0272
BS900	56.22	28.80	0.0133	0.0166
CS500	76.30	13.73	0.0064	0.0253
CS600	464.66	264.10	0.1074	0.1526
CS700	448.50	317.69	0.1254	0.1468
CS800	49.79	40.44	0.0154	0.0161
CS900	32.20	22.06	0.0087	0.0095
PS500	77.33	64.56	0.0246	0.0241
PS600	319.02	226.71	0.0894	0.1013
PS700	267.84	104.43	0.0474	0.0871
PS800	117.37	68.01	0.0277	0.0384
PS900	79	62.76	0.0240	0.0248
RS500	6.54	0.11	0.0003	0.0021
RS600	23.11	7.38	0.0034	0.0077
RS700	45.98	16.33	0.0075	0.0151
RS800	34.36	16.48	0.0076	0.0114
RS900	29.94	17.66	0.0072	0.0105

S_{BET}: The specific surface area was obtained by the BET model.
S_{mic}: The micropore surface area was obtained by the t-Plot model.
V_{mic}: The micropore volume was obtained by the DFT model.
V_{total}: Pore volume was estimated at P/P0 = 0.99.

Despite differences in specific surface areas among the five biomass samples, they generally show similar patterns. Most samples experience a notable increase in specific surface area and pore volume as the temperature rises from 500℃ to 600℃, with the exception of rice straw. Higher temperatures lead to the evaporation of more volatile compounds, resulting in larger pore volumes and consequently greater surface areas. Peanut shells and coconut shells can reach a maximum of 600°C, bamboo slice and rice stalks can reach 700°C, and poplar wood can reach 800°C. However, as the temperature continues to rise, the surface area decreases. The reactivity of biochar samples is strongly influenced by their surface area.[98], so biochar produced in the 600°C-800°C temperature range exhibits better reactivity and adsorption behavior. PW800 demonstrates excellent performance across all metrics and holds significant potential for future applications. Therefore, poplar wood was selected for the subsequent activation experiment.

4.4 Properties of activated samples

4.4.1 Fourier transform infrared spectrum of activated biochar (FT-IR)

The FTIR spectrum of activated biochar produced by pyrolysis of poplar at 800°C is shown in Figure 4.14. Significant changes in the absorption peaks of poplar biochar after activation are observed. The stretching vibrations of AKP800 at 3500 cm^{-1} and 2700 cm^{-1} were observed to assign C-H bonds to hydroxyl (-OH) groups and alkane groups from carboxyl, phenolic or alcohol, and adsorbable water. Additionally, peaks associated with carboxyl groups (C=O) were identified in the range of 2000-1750 cm^{-1} for both BKP800 and AKP800. The band at 1650 is considered to be the stretching vibration of aryl C=C, and the strong broad peaks around 1400-1000cm^{-1} represent the stretching of C-O-C glycosidic bond. Compared with FTIR of PW800 before activation (Figure 4.4), the absorption peak of the -OH functional group of AKP800 was

significantly enhanced. This is because KOH is a strong base, and when it reacts with biomass at high temperatures, it will lead to complex chemical reactions, especially dehydrogenation reactions with lignin and cellulose in biomass. KOH not only increases the specific surface area as a physical activator, but also induces the formation of surface -OH. The mechanism includes the free radicals produced during oxidation and activation, which introduce more hydroxyl functional groups on the surface of biochar. It is also possible that the KOH activation process greatly improves the specific surface area and pore structure, providing reaction sites for the formation of more -OH groups. However, no significant -OH and C-H vibrations were observed in BKP800, which is because some soluble organic and hydroxyl functional groups were removed by ionic washing before pyrolysis. During the pyrolysis process, poplar wood needs to consume excessive -OH in KOH to form a porous carbon framework, and the carbonisation structure is relatively stable and it is difficult to introduce new hydroxyl groups. The reduction in C-H group strength is due to the conversion of the benzene ring's three-dimensional network into a two-dimensional gelled ring structure, achieved by breaking methyl, methylene, and oxygen-containing functional groups. This structure subsequently transforms into a graphite microcrystalline form through molten ring expansion and dehydrogenation[99]. Moreover, the presence of elevated C=O, C=C, and C-O-C functional groups in both AKP800 and BKP800 is more pronounced compared to PW800, which suggests these groups could supply additional adsorption sites.

After KOH modification, the peak intensities of AKP800 and BKP800 increased significantly compared to PW800, indicating that KOH activation promotes the formation of surface functional groups in biochar. AKP800 contains more functional groups than BKP800, resulting in superior adsorption performance. Adsorption capacity of biochar is greatly enhanced by oxygen-containing functional groups [100].

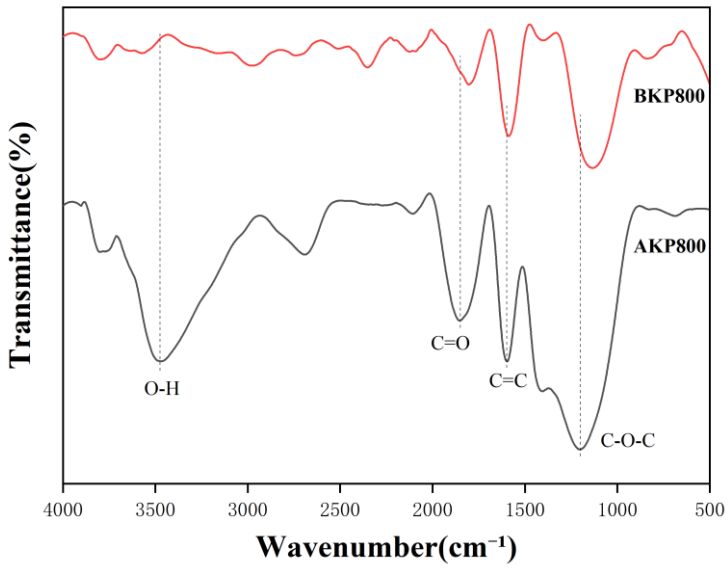

Figure 4.14 FTIR spectra of poplar biochar activated from KOH.

4.4.2 Scanning electron microscopy of activated biochar (SEM)

The surface morphology of activated biochar was observed using scanning electron microscopy (SEM) (Figure 4.15), and the elemental distribution on the surface of both biochar samples was examined with energy dispersive X-ray spectroscopy (EDS). Compared to PW800, biochar samples activated with KOH exhibit a more developed pore structure, offering a larger specific surface area and pore volume. As shown in Figure 4.15 (b), BKP800 contains irregularly distributed pores and a relatively smooth surface, while AKP800 features smaller, more abundant pores and a relatively rough surface. The addition of KOH solution promotes reactions during pyrolysis, releasing more gases and enlarging the pores, thus increasing pore abundance. Based on SEM image results, Figure 4.15 (a) demonstrates a more developed pore structure, larger specific surface area, and greater pore volume, suggesting that AKP800 has higher potential for medical applications.

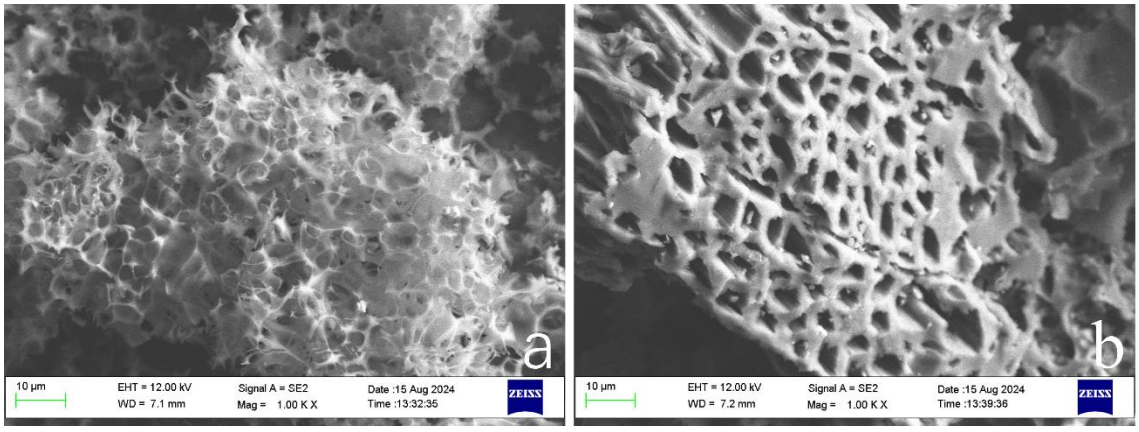

Figure 4.15 SEM images of (a) AKP800, (b)BKP800.

EDS studies were conducted in parallel with SEM analysis to examine the trace chemical composition of the biochar surface. As shown in Table 4.6, the primary chemical components of AKP800 and BKP800 are carbon and oxygen. The presence of these elements is attributed to the cellulose, hemicellulose, and lignin found in the biomass. The carbon content of PW800 is 80.22%. After activation, the carbon content of AKP800 and BKP800 increased to 85.81% and 89.83%. However, compared with PW800 (12.5%), the oxygen content of AKP800 (13.75%) was increased and that of BKP800 (8.58%) was decreased. The element is bound as a surface oxygen group, which is consistent with the conclusion in FTIR (Figure 4.14). The presence of other elements, such as Mg and Ca in AKP800, is largely influenced by the chemical composition of the biomass, while K (1.59%) in BKP800 may be residual after cleaning with deionized water prior to pyrolysis.

Table 4.6 EDS analysis of activated biochar

Element	C (%)	O (%)	K (%)	Ca (%)	Mg (%)
AKP800	85.81	13.75	0	0.27	0.17
BKP800	89.83	8.58	1.59	0	0

4.4.3 Specific surface area of activated biochar (BET)

Figure 4.16 displays the N_2 adsorption-desorption isotherm, which was categorized according to the classification system established by the International Union of Pure and Applied Chemistry (IUPAC). The adsorption curves of AKP800 and BKP800 both

exhibit a type I shape (Figure 4.18 (a)). When P/Po < 0.1, N_2 adsorption increases rapidly, and the plateaus are fairly flat, indicating a high concentration of micropores. As the relative pressure increases, an H4 hysteresis loop appears on the adsorption-desorption curve (Figure 4.18 (b)), which is characteristic of active biochar solids with narrow slit-like pores[101], suggesting a notable increase in pore size. The pore size distribution of the biochar was calculated using the DFT method. According to the IUPAC standards, pores are classified into three categories: micropores (< 2 nm), mesopores (2-50 nm), and macropores (> 50 nm). Figure 4.17 shows that biochar activated by KOH is rich in micropores, confirming that the prepared active biochar is a microporous material. The analysis of pore distribution and specific surface area reveals that pore size and volume are interdependent, influencing the specific surface area of biochar. A smaller pore diameter results in a higher specific surface area due to the increased number of microscopic pores in confined spaces. Table 4.7 provides a summary of the specific surface area, total pore volume, and average pore diameter for AKP800 and BKP800. The surface area of AKP800 notably rises to 2028.96 m^2/g, surpassing both BKP800 (1042.86 m^2/g) and PW800 (451.06 m^2/g). It also exceeds previous studies[102]. The total pore volume also increased to 0.7379 cm^3/g, and AKP800 showed excellent performance in all aspects, indicating that KOH activation significantly enhanced the surface properties of biochar.

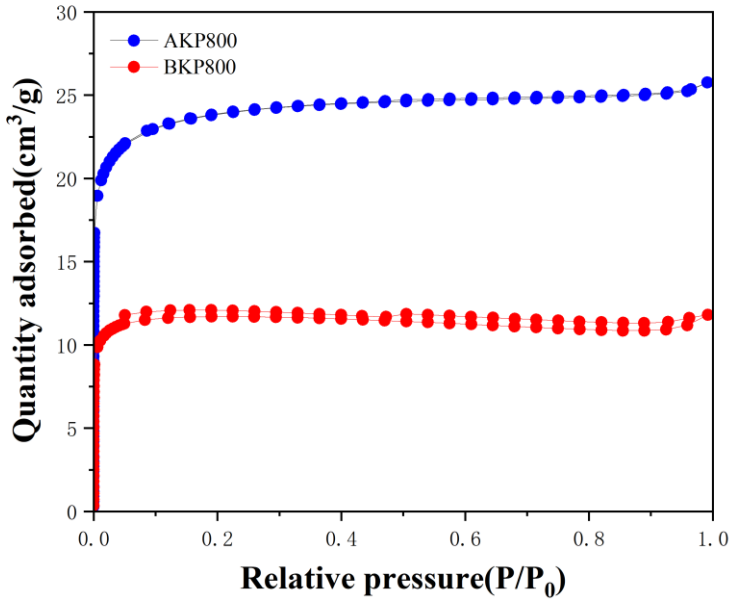

Figure 4.16 N_2 adsorption-desorption isotherm of biochar AKP800 and BKP800.

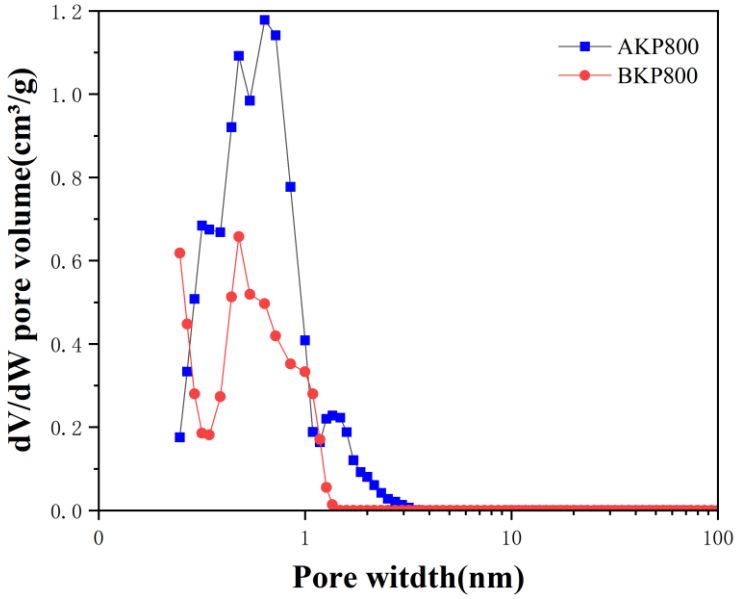

Figure 4.17 Pore size distribution of biochar AKP800 and BKP800 by DFT model.

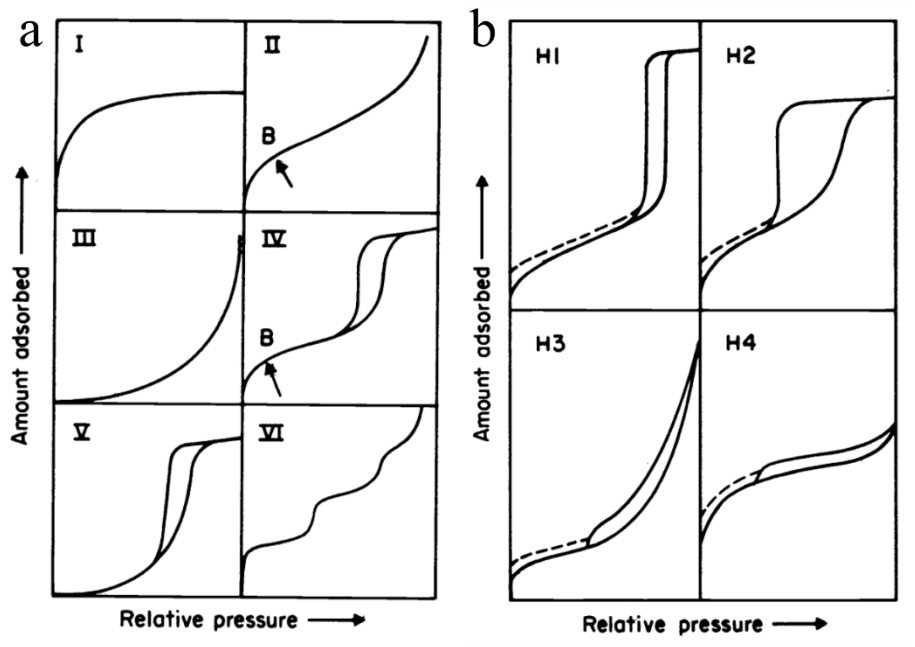

Figure 4.18 Types of physical adsorption isotherms (a) and types of desorption hysteresis loops (b)[103]

The method for constructing a porous structure in poplar wood powder involves two stages: a low-temperature activation stage and a high-temperature activation stage. The first stage, or pre-activation stage, facilitates the uniform incorporation of potassium into the biomass, while the activator undergoes dehydration and transforms into the active component responsible for pore formation. During the activation process, only steam is produced, indicating that a microporous activation reaction is unlikely at this stage. The oxygen groups on the surface of the raw material interact with the alkali activator, and the primary reaction involves the dehydration of the activation centre. The main reactions are as follows[104]:

$$2\,\mathrm{KOH} \rightarrow K_2O + H_2O \tag{10}$$

$$-\mathrm{OH} + \mathrm{KOH} \rightarrow -\mathrm{OK} + H_2O \tag{11}$$

$$-\mathrm{COOH} + \mathrm{KOH} \rightarrow -\mathrm{COOK} + H_2O \tag{12}$$

In the second stage, as the pyrolysis temperature increases, the carbon-based groups in the powder skeleton begin to react and volatilise in gaseous form. Under high-temperature conditions, organic components such as hydrogen, oxygen, and nitrogen are produced, causing these elements in the organic matter to decompose continuously.

The well-distributed KOH ensures the homogeneity of its reaction with all carbon surfaces within the carbon network, and the carbon atoms are continuously cyclized and aromatised. Hydrogen, oxygen, nitrogen and other atoms continue to reduce, carbon continues to enrich, and caves appear in the original location, thus forming new pores. In addition, KOH etches carbon fragments and reacts with oxygen in the activation products to release gaseous products and form a large number of pores. The rich functional groups in biomass are also degraded in the presence of KOH into volatiles such as water and carbon dioxide, which are released through the structure of carbon, thus forming pores. In addition, the biological carbon reacts with potassium carbonate or potassium oxide, resulting in pore formation or expansion of existing pores. During the washing of deionized water, the potassium compounds embedded in the carbon structure (K_2O, K_2CO_3 and K) are eliminated, resulting in activated carbon with high surface area and high porosity[105]. KOH can also dissolve ash and condense organic matter (such as cellulose and lignin) to facilitate subsequent activation[106]. Therefore, possible reactions are as follows[107]:

$$-CH_2 + 4\,\mathrm{KOH} \rightarrow K_2CO_3 + K_2O + 3\,H_2 \quad (13)$$

$$2-\mathrm{CH} + 8\,\mathrm{KOH} \rightarrow 2\,K_2CO_3 + 2\,K_2O + 5\,H_2 \quad (14)$$

$$4\,\mathrm{KOH} + \mathrm{C} \rightarrow K_2CO_3 + K_2O + 2\,H_2 \quad (15)$$

$$K_2CO_3 + 2\,\mathrm{C} \rightarrow K_2O + 2\,\mathrm{CO} \quad (16)$$

$$K_2O + \mathrm{C} \rightarrow 2\,\mathrm{K} + \mathrm{CO} \quad (17)$$

KOH promotes volatilisation reactions and chemical etching within the dense carbon network, which decompose more rapidly at elevated temperatures, leading to an increase in pore volume and surface area. Since the objective of these studies is to produce biochar with a high specific surface area, the S_{BET} value is a critical factor. This goal was achieved by obtaining AKP800 through the pyrolysis of activated poplar wood at the optimal temperature. The results indicate that KOH plays a significant role in developing porous structures, enabling the production of biochar with excellent structural parameters, high specific surface area, and microporosity.

Table 4.7 Pore parameters of activated biochar

Samples	Ash	Specific Surface Area	Total Volume Pore	Mean hole radius
	(%)	S_{BET} (m^2/g)	V_{total} (cm^3/g)	R_m (nm)
AKP800	2.44	2028.96	0.7379	1.7638
BKP800	1.69	1042.86	0.3310	1.5737

S_{BET}: The specific surface area was obtained by the BET model.

V_{total}: Pore volume was estimated at $P/P_0 = 0.99$.

R_m: The mean hole radius was obtained by the BJH model.

4.5 Relationship between temperature, lignocellulose and specific surface area

A series of experiments demonstrated that pyrolysis temperature is a key factor in determining the specific surface area of biochar. For instance, Figure 4.19 illustrates the changes in the specific surface area of poplar wood, bamboo slices, coconut shells, peanut shells, and rice straw as the temperature increases from 500°C to 900°C. The surface area of biochar increases with rising temperature but decreases after reaching the optimal temperature. With increasing heat treatment temperatures, volatile substances are released and pores are formed. In addition to forming vascular bundles and channels, the gradual degradation of organic materials (cellulose, lignin) increases surface area and pore volume. During the pyrolysis process, some amorphous carbon structures are also formed along with increased micropore numbers. Carbon structures with amorphous compositions have been reported to form micropores[108]. Therefore, CS (464.66 m^2/g) and PS (319.02 m^2/g) at 600℃, BS (252.18 m^2/g) and RS (45.98 m^2/g) at 700℃, and PW (451.06 m^2/g) at 800℃ all show the largest specific surface area. However, continued warming results in a decrease in surface area. This is due to the collapse, deformation, contraction or blockage of micropore structures in biochar. In addition, some carbon structures may order and merge pores, thereby reducing the surface area of the carbon[109]. The results show that the pyrolysis temperature has a

great influence on the pore structure of the material, and 600℃-800℃ is the best temperature for producing high specific surface area, which proves that high temperature carbonisation is a promising way to prepare biochar with good porosity.

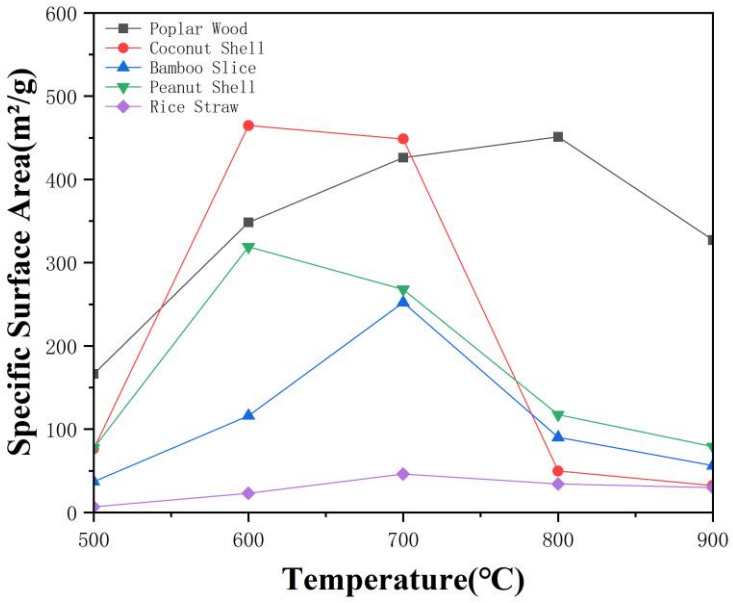

Figure 4.19 The specific surface area of biochar produced by each biomass at different.

However, RS (41.83 m^2/g) exhibits the smallest specific surface area at all temperatures. The results show that a high cellulose content is more conducive to the production of biochar with a high specific surface area (Figure 4.20), which is consistent with previous studies[110]. By dehydration, decarboxylation, aromatisation and intramolecular condensation, cellulose char is derived from the linear homopolysaccharide cellobiose monomer. In pyrolysis, cellulose creates secondary char, which is classified as carbon. Amorphous carbon forms micropores as a result of the release of large quantities of non-condensable gases during secondary pyrolysis. Consequently, the breakdown of cellulose generates additional micropores in the biochar, increasing its specific surface area. The cellulose content of BS (46.54%) and PS (45.22%) was similar, but the maximum surface area of PS (319.02 m^2/g) was significantly larger than that of BS (252.18 m^2/g). This may be related to their lignin content (Table 4.3). The lignin content of PS is as high as 31.47%, which is higher than

that of BS (19.36%). The further degradation of lignin and the aromatic condensation reaction increased the release of volatile substances and produced more pores. At the same time, the decomposition of lignin and the rapid release of H_2 and CH_4 greatly increase the specific surface area and pore volume[111]. The content of cellulose and lignin in RS is low, and the ash content (24.46%-27.69%) in RS is significantly higher than that in other biochar. The lower surface area may also be the result of molten ash blocking the pores in the biochar (Figure 4.13). Therefore, for the production of biochar with large specific surface area, it is recommended to choose biomass with high cellulose and lignin content and low ash content for pyrolysis.

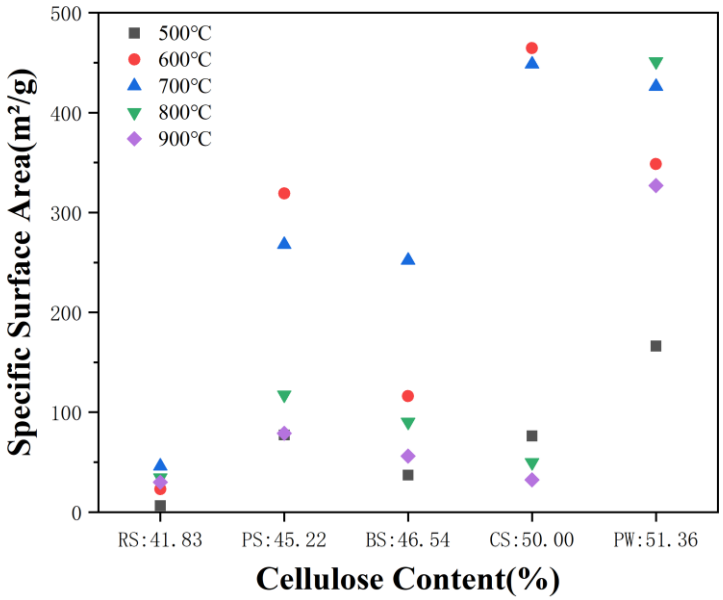

Figure 4.20 The relationship between the content of cellulose and the specific surface area of biochar prepared at different pyrolysis temperatures.

5. CONCLUSIONS AND PROSPECT

In this study, biochar pyrolysis from five different biomass sources including poplar (PW), bamboo slice (BS), coconut shell (CS), peanut shell (PS) and rice straw (RS) was analysed comprehensively. The results showed that the chemical composition of biomass and pyrolysis conditions greatly determined the final properties of biochar, especially the KOH activation process significantly improved the specific surface area and pore structure of biochar. With the increase of pyrolysis temperature, the hydrogen-carbon atom ratio (H/C) decreased significantly, and the biochar changed from a hydrocarbon structure to a more stable aromatic carbon structure, which increased the antioxidant energy of biochar. Similarly, the oxygen-carbon ratio (O/C) also decreases with increasing temperature, reflecting a decrease in biochar polarity. Furthermore, as the temperature rises, the absorption peaks associated with hydroxyl (OH) and carbonyl (C=O) groups diminish markedly, leading to the formation of more stable aromatic compounds. The specific surface area of biochar is a key parameter for its potential use in adsorption-based applications, and this study shows that the specific surface area increases first and then decreases, with an optimal temperature range between 600℃ and 800℃. Biomass with high cellulose content, such as poplar wood and coconut shell, has a larger biochar specific surface area. The decomposition of lignin also has a positive effect on the relative surface area, but high ash content will clog the pores and reduce the specific surface area. Therefore, it is easy to obtain high-quality biochar with high stability, high specific surface area and rich pore structure after pyrolysis of biomass with high cellulose lignin content at the optimal temperature.

In the process of this experiment, appropriate activator (KOH) was used to optimise the microstructure of biochar. Specifically, KOH significantly enhances the porosity and specific surface area of biochar by chemically etching and promoting volatile reactions during activation. The prepared specific surface area reached a record 2028.96 m^2/g, exceeding most commercial biochar on the market. The absorption peaks of surface functional groups, such as carboxyl group (C=O) and hydroxyl group (-OH), were also

significantly enhanced. As a result, these functional groups on the surface of biochar provide more active sites for the adsorption process and further enhance its adsorption capacity.

In summary, this study highlights the importance of the relationship between the chemical composition of biomass and the properties of the resulting biochar. The potential to obtain superior biochar from a variety of biomass sources through controlled pyrolysis and activation processes has been successfully demonstrated. These findings not only contribute to the understanding of biochar production but also provide a solid theoretical foundation for the future development of biochar as a functional material, especially in the biomedical field. The material's unique porous architecture combined with tunable surface chemistry renders it particularly suitable for drug delivery system construction. The extensive specific surface area enables sufficient drug molecule loading, while the hierarchical porosity facilitates controlled drug release. Surface modification enhances both biocompatibility and targeting capabilities, enabling precise delivery of antitumor and antibacterial therapeutics. The material's high surface area and abundant active sites significantly improve biosensor detection sensitivity, particularly for real-time blood glucose monitoring and rapid viral detection.

However, there are still many deficiencies in the study of biochar adsorption capacity and toxicity. Therefore, it is also necessary to verify its mechanism through a series of experiments to lay a good foundation for future application. There is also a need to address the scalability of biochar production and its economic viability to promote widespread adoption. This will not only help promote the practical application of biochar in various fields, but also play a positive role in promoting the realisation of the global sustainable development goals.

REFERENCES

[1]Adepu, S. and Ramakrishna, S., 2021. Controlled drug delivery systems: current status and future directions. *Molecules*, *26*(19), p.5905.

[2]Zhang, L., Xu, C.C. and Champagne, P., 2010. Overview of recent advances in thermo-chemical conversion of biomass. Energy conversion and management, 51(5), pp.969-982.

[3]Chum, H.L. and Overend, R.P., 2001. Biomass and renewable fuels. Fuel processing technology, 71(1-3), pp.187-195.

[4]Laine, C., 2005. Structures of hemicelluloses and pectins in wood and pulp. Helsinki University of Technology.

[5]Lee, H.V., Hamid, S.B.A. and Zain, S.K., 2014. Conversion of lignocellulosic biomass to nanocellulose: structure and chemical process. The Scientific World Journal, 2014(1), p.631013.

[6]Himmel, M.E., Ding, S.Y., Johnson, D.K., Adney, W.S., Nimlos, M.R., Brady, J.W. and Foust, T.D., 2007. Biomass recalcitrance: engineering plants and enzymes for biofuels production. science, 315(5813), pp.804-807.

[7]Lam, S.S., Mahari, W.A.W., Ok, Y.S., Peng, W., Chong, C.T., Ma, N.L., Chase, H.A., Liew, Z., Yusup, S., Kwon, E.E. and Tsang, D.C., 2019. Microwave vacuum pyrolysis of waste plastic and used cooking oil for simultaneous waste reduction and sustainable energy conversion: Recovery of cleaner liquid fuel and techno-economic analysis. Renewable and Sustainable Energy Reviews, 115, p.109359.

[8]Zhang, Q., Xiao, J., Xue, J. and Zhang, L., 2020. Quantifying the effects of biochar application on greenhouse gas emissions from agricultural soils: a global meta-analysis. Sustainability, 12(8), p.3436.

[9]Lehmann, J. and Joseph, S. eds., 2024. Biochar for environmental management: science, technology and implementation. Taylor & Francis.

[10]Woolf, D., Amonette, J.E., Street-Perrott, F.A., Lehmann, J. and Joseph, S., 2010. Sustainable biochar to mitigate global climate change. Nature communications, 1(1), p.56.

[11]Kung, C.C. and Chang, M.S., 2015. Effect of agricultural feedstock to energy conversion rate on bioenergy and GHG emissions. Sustainability, 7(5), pp.5981-5995.

[12]Jindo, K., Mizumoto, H., Sawada, Y., Sanchez-Monedero, M.A. and Sonoki, T., 2014. Physical and chemical characterization of biochars derived from different agricultural residues. Biogeosciences, 11(23), pp.6613-6621.

[13]Ortiz, L.R., Torres, E., Zalazar, D., Zhang, H., Rodriguez, R. and Mazza, G., 2020. Influence of pyrolysis temperature and bio-waste composition on biochar characteristics. Renewable Energy, 155, pp.837-847.

[14]Liu, M., Almatrafi, E., Zhang, Y., Xu, P., Song, B., Zhou, C., Zeng, G. and Zhu, Y., 2022. A critical review of biochar-based materials for the remediation of heavy metal contaminated environment: Applications and practical evaluations. Science of the Total Environment, 806, p.150531.

[15]Patel, A.K., Katiyar, R., Chen, C.W., Singhania, R.R., Awasthi, M.K., Bhatia, S., Bhaskar, T. and Dong, C.D., 2022. Antibiotic bioremediation by new generation biochar: recent updates. Bioresource Technology, 358, p.127384.

[16]Xu, K., Zhang, C., Dou, X., Ma, W. and Wang, C., 2019. Optimizing the modification of wood waste biochar via metal oxides to remove and recover phosphate from human urine. Environmental geochemistry and health, 41, pp.1767-1776.

[17]Li, J., Qiao, Y., Zong, P., Qin, S., Wang, C. and Tian, Y., 2019. Fast pyrolysis characteristics of two typical coastal zone biomass fuels by thermal gravimetric analyzer and down tube reactor. Bioresource technology, 283, pp.96-105.

[18]Turrado Fernández, S., Paredes Sánchez, J.P. and Gutiérrez Trashorras, A.J., 2016. Analysis of forest residual biomass potential for bioenergy production in Spain. Clean Technologies and Environmental Policy, 18, pp.209-218.

[19]Nguyen, N.V. and Trinh, H.L., 2020. Determination of water quality parameters in the Tan Rai exploiting area (Lam Dong province) using Sentinel-2 MSI and Landsat 8 data. Journal of Mining and Earth Sciences, 61(2), pp.126-134.

[20]Muhammad, N., Nafees, M., Khan, M.H., Ge, L. and Lisak, G., 2020. Effect of biochars on bioaccumulation and human health risks of potentially toxic elements in wheat (Triticum aestivum L.) cultivated on industrially contaminated soil. Environmental Pollution, 260, p.113887.

[21]Ma, Y., Zhang, T., Zhu, P., Cai, H., Jin, Y., Gao, K. and Li, J., 2022. Fabrication of Ag3PO4/polyaniline-activated biochar photocatalyst for efficient triclosan degradation process and toxicity assessment. Science of The Total Environment, 821, p.153453.

[22]Zhuo, Q., Liang, Y., Hu, Y., Shi, M., Zhao, C. and Zhang, S., 2023. Applications of biochar in medical and related environmental fields: current status and future

perspectives. Carbon Research, 2(1), p.32.

[23]Pariyar, P., Kumari, K., Jain, M.K. and Jadhao, P.S., 2020. Evaluation of change in biochar properties derived from different feedstock and pyrolysis temperature for environmental and agricultural application. Science of the Total Environment, 713, p.136433.

[24]Ambaye, T.G., Vaccari, M., van Hullebusch, E.D., Amrane, A. and Rtimi, S.J.I.J.O.E.S., 2021. Mechanisms and adsorption capacities of biochar for the removal of organic and inorganic pollutants from industrial wastewater. International Journal of Environmental Science and Technology, 18(10), pp.3273-3294.

[25]Amenaghawon, A.N., Anyalewechi, C.L., Okieimen, C.O. and Kusuma, H.S., 2021. Biomass pyrolysis technologies for value-added products: a state-of-the-art review. Environment, development and sustainability, pp.1-55.

[26]Yu, J., Paterson, N., Blamey, J. and Millan, M., 2017. Cellulose, xylan and lignin interactions during pyrolysis of lignocellulosic biomass. Fuel, 191, pp.140-149.

[27]Pandey, D., Daverey, A. and Arunachalam, K., 2020. Biochar: Production, properties and emerging role as a support for enzyme immobilization. Journal of Cleaner Production, 255, p.120267.

[28]Chen, D., et al., 2015. Torrefaction of biomass stalk and its effect on the yield and quality of pyrolysis products. Fuel, 159: p. 27-32.

[29]Si, H.P., et al., 2015. Review on pyrolysis carbonization technology of biomass. Advanced Materials Research, 1092: p. 72-78.

[30]Khosravanipour Mostafazadeh, A., et al., 2018. A review of recent research and developments in fast pyrolysis and bio-oil upgrading. Biomass Conversion Biorefinery, 8: p. 739-773.

[31]O'Laughlin, J. and McElligott, K., 2009. 'Biochar for environmental management: science and technology', in Lehmann, J. and Joseph, S.M. (eds.) Biochar for Environmental Management: Science and Technology. London: Earthscan, pp. 448.

[32]Van Zwieten, L., et al., 2010. Effects of biochar from slow pyrolysis of papermill waste on agronomic performance and soil fertility. Plant soil, 327: p. 235-246.

[33]Chen, W., et al., 2019. Past, present, and future of biochar. Biochar, 1: p. 75-87.

[34]Zhang, Z., et al., 2021. Biowaste hydrothermal carbonization for hydrochar valorization: Skeleton structure, conversion pathways and clean biofuel applications. Bioresource technology, 324: p. 124686.

[35]Wei, J., et al., 2019. Assessing the effect of pyrolysis temperature on the molecular properties and copper sorption capacity of a halophyte biochar. Environmental Pollution, 251: p. 56-65.

[36]Zhao, S.-X., N. Ta, and X.-D. Wang, 2017. Effect of temperature on the structural and physicochemical properties of biochar with apple tree branches as feedstock material. Energies. 10(9): p. 1293.

[37]Yuan, T., et al., 2020. Comparison of bio-chars formation derived from fast and slow pyrolysis of walnut shell. Fuel, 261: p. 116450.

[38]Pecha, M.B., et al., 2019. Progress in understanding the four dominant intra-particle phenomena of lignocellulose pyrolysis: chemical reactions, heat transfer, mass transfer, and phase change. Green chemistry, 21(11): p. 2868-2898.

[39]Varma, A.K., et al., 2019. Pyrolysis of wood sawdust: Effects of process parameters on products yield and characterization of products. Waste Management, 89: p. 224-235.

[40]Zhang, J., J. Liu, and R. Liu, 2015. Effects of pyrolysis temperature and heating time on biochar obtained from the pyrolysis of straw and lignosulfonate. Bioresource Technology, 176: p. 288-291.

[41]Sun, J., et al., 2017. Effects of pyrolysis temperature and residence time on physicochemical properties of different biochar types. Acta Agriculturae Scandinavica, Section B—Soil & Plant Science, 67(1): p. 12-22.

[42]Kumar, P., et al., 2009. Methods for pretreatment of lignocellulosic biomass for efficient hydrolysis and biofuel production. Industrial engineering chemistry research, 48(8): p. 3713-3729.

[43]Shi, R.-y., et al., 2018. Peanut straw biochar increases the resistance of two Ultisols derived from different parent materials to acidification: A mechanism study. Journal of environmental management. 210: p. 171-179.

[44]Suliman, W., et al., 2016. Influence of feedstock source and pyrolysis temperature on biochar bulk and surface properties. Biomass Bioenergy 84: p. 37-48.

[45]Yoo, S., et al., 2018. Structural characterization of loblolly pine derived biochar by X-ray diffraction and electron energy loss spectroscopy. ACS Sustainable Chemistry Engineering 6(2): p. 2621-2629.

[46]Dawood, S., T.K. Sen, and C. Phan, 2017. Synthesis and characterization of slow pyrolysis pine cone bio-char in the removal of organic and inorganic pollutants from aqueous solution by adsorption: kinetic, equilibrium, mechanism and thermodynamic.

Bioresource Technology 246: p. 76-81.

[47]Kalderis, D., et al., 2017. Adsorption of 2, 4-dichlorophenol on paper sludge/wheat husk biochar: Process optimization and comparison with biochars prepared from wood chips, sewage sludge and hog fuel/demolition waste. Journal of environmental chemical engineering 5(3): p. 2222-2231.

[48]Uchimiya, M., Chang, S. and Klasson, K.T., 2011. Screening biochars for heavy metal retention in soil: role of oxygen functional groups. Journal of Hazardous Materials, 190(1-3), pp.432-441.

[49]Hadjittofi, L., Prodromou, M. and Pashalidis, I., 2014. Activated biochar derived from cactus fibres–preparation, characterization and application on Cu (II) removal from aqueous solutions. Bioresource technology, 159, pp.460-464.

[50]Mahmoud, D.K., et al., 2012. Batch adsorption of basic dye using acid treated kenaf fibre char: Equilibrium, kinetic and thermodynamic studies. Chemical Engineering Journal, 181: p. 449-457.

[51]Jin, H., et al., 2014. Biochar pyrolytically produced from municipal solid wastes for aqueous As (V) removal: adsorption property and its improvement with KOH activation. Bioresource technology, 169: p. 622-629.

[52]Pietrzak, R., et al., 2014. Comparison of the effects of different chemical activation methods on properties of carbonaceous adsorbents obtained from cherry stones. Chemical Engineering Research Design, 92(6): p. 1187-1191.

[53]Dehkhoda, A.M., Gyenge, E. and Ellis, N., 2016. A novel method to tailor the porous structure of KOH-activated biochar and its application in capacitive deionization and energy storage. Biomass and Bioenergy, 87, pp.107-121.

[54]Galhetas, M., et al., 2014. Chars from gasification of coal and pine activated with K_2CO_3: Acetaminophen and caffeine adsorption from aqueous solutions. Journal of Colloid Interface Science, 433: p. 94-103.

[55]Liu, W.-J., H. Jiang, and H.-Q. Yu, 2015.Development of biochar-based functional materials: toward a sustainable platform carbon material. Chemical reviews, 115(22): p. 12251-12285.

[56]Zhao, C., et al., 2023. Effects of cellulose addition on the physicochemical properties, pore structure and iodine adsorption of lignin-based biochar. Fuel, 352: p. 129061.

[57]Li, J., et al., 2020. Catalytic conversion of gaseous tars using land, coastal and

marine biomass-derived char catalysts in a bench-scale downstream combined fixed bed system. Bioresource technology, 304: p. 122735.

[58]Yousaf, B., et al., 2017. Investigating the biochar effects on C-mineralization and sequestration of carbon in soil compared with conventional amendments using the stable isotope (δ13C) approach. Gcb Bioenergy, 9(6): p. 1085-1099.

[59]Ahmad, M., et al., 2014. Biochar as a sorbent for contaminant management in soil and water: a review. Chemosphere, 99: p. 19-33.

[60]Nanda, S., et al., 2016. Biochar as an exceptional bioresource for energy, agronomy, carbon sequestration, activated carbon and specialty materials. Waste Biomass Valorization, 7: p. 201-235.

[61]Dong, X., et al., 2018. Preparation of highly conductive biochar nanoparticles for rapid and sensitive detection of 17β-estradiol in water. Electrochimica Acta, 292: p. 55-62.

[62]Li, Y., et al., 2022. Recent advances of biochar-based electrochemical sensors and biosensors. Biosensors, 12(6): p. 377.

[63]Kalinke, C., et al., 2019. Green method for glucose determination using microfluidic device with a non-enzymatic sensor based on nickel oxyhydroxide supported at activated biochar. Talanta, 200: p. 518-525.

[64]Cancelliere, R., et al., 2022. Cost-effective and disposable label-free voltammetric immunosensor for sensitive detection of interleukin-6. Biosensors Bioelectronics, 213: p. 114467.

[65]Wang, F., et al., 2021. Lollipop-inspired multilayered drug delivery hydrogel for dual effective, long-term, and NIR-defined glaucoma treatment. Macromolecular Bioscience, 21(11): p. 2100202.

[66]Pang, Y.X., Sharmin, N., Wu, T. and Pang, C.H., 2023. An investigation on plant cell walls during biomass pyrolysis: A histochemical perspective on engineering applications. Applied Energy, 343, p.121055.

[67]Isikgor, F.H. and Becer, C.R., 2015. Lignocellulosic biomass: a sustainable platform for the production of bio-based chemicals and polymers. Polymer chemistry, 6(25), pp.4497-4559.

[68]Fahmi, R., Bridgwater, A.V., Donnison, I., Yates, N. and Jones, J.M., 2008. The effect of lignin and inorganic species in biomass on pyrolysis oil yields, quality and stability. Fuel, 87(7), pp.1230-1240.

[69]Jenkins, M.B., et al., 1998. Combustion Properties of Biomass. Fuel Process. Technol. 54,17.

[70]Tian, X., Wang, Y., Zeng, Z., Dai, L., Peng, Y., Jiang, L., Yang, X., Yue, L., Liu, Y. and Ruan, R., 2021. Study on the mechanism of co-catalyzed pyrolysis of biomass by potassium and calcium. Bioresource Technology, 320, p.124415.

[71]Arvelakis, S., Gehrmann, H., Beckmann, M. and Koukios, E.G., 2002. Effect of leaching on the ash behavior of olive residue during fluidized bed gasification. Biomass and Bioenergy, 22(1), pp.55-69.

[72]Yu, H., Wu, Z. and Chen, G., 2018. Catalytic gasification characteristics of cellulose, hemicellulose and lignin. Renewable Energy, 121, pp.559-567.

[73]Bosch, M. and Hazen, S.P., 2013. Lignocellulosic feedstocks: research progress and challenges in optimizing biomass quality and yield. Frontiers in Plant Science, 4, p.474.

[74]Lobos, M.L.N., Sieben, J.M., Comignani, V., Duarte, M., Volpe, M.A. and Moyano, E.L., 2016. Biochar from pyrolysis of cellulose: an alternative catalyst support for the electro-oxidation of methanol. international journal of hydrogen energy, 41(25), pp.10695-10706.

[75]Zhang, T., Wyman, C.E., Jakob, K. and Yang, B., 2012. Rapid selection and identification of Miscanthus genotypes with enhanced glucan and xylan yields from hydrothermal pretreatment followed by enzymatic hydrolysis. Biotechnology for biofuels, 5, pp.1-14.

[76]Song, F., Li, T., Zhang, J., Wang, X., Bai, Y., Giesy, J.P., Xing, B. and Wu, F., 2019. Novel insights into the kinetics, evolved gases, and mechanisms for biomass (sugar cane residue) pyrolysis. Environmental Science & Technology, 53(22), pp.13495-13505.

[77]Neves, D., Thunman, H., Matos, A., Tarelho, L. and Gómez-Barea, A., 2011. Characterization and prediction of biomass pyrolysis products. Progress in energy and combustion Science, 37(5), pp.611-630.

[78]Chen, B., Zhou, D. and Zhu, L., 2008. Transitional adsorption and partition of nonpolar and polar aromatic contaminants by biochars of pine needles with different pyrolytic temperatures. Environmental science & technology, 42(14), pp.5137-5143.

[79]Wang, X., Guo, Z., Hu, Z. and Zhang, J., 2020. Recent advances in biochar application for water and wastewater treatment: a review. PeerJ, 8, p.e9164.

[80]Jamal, M.U. and Fletcher, A.J., 2023. Design of experiments study on Scottish

wood biochars and process parameter influence on final biochar characteristics. BioEnergy Research, 16(4), pp.2342-2355.

[81]Patel, M., Kumar, R., Pittman Jr, C.U. and Mohan, D., 2021. Ciprofloxacin and acetaminophen sorption onto banana peel biochars: Environmental and process parameter influences. Environmental Research, 201, p.111218.

[82]Greenwood, P.F., Van Heemst, J.D., Guthrie, E.A. and Hatcher, P.G., 2002. Laser micropyrolysis GC–MS of lignin. Journal of Analytical and Applied Pyrolysis, 62(2), pp.365-373.

[83]Liu, Q., Wang, S., Zheng, Y., Luo, Z. and Cen, K., 2008. Mechanism study of wood lignin pyrolysis by using TG–FTIR analysis. Journal of analytical and applied pyrolysis, 82(1), pp.170-177.

[84]Zhuang, J., Li, M., Pu, Y., Ragauskas, A.J. and Yoo, C.G., 2020. Observation of potential contaminants in processed biomass using fourier transform infrared spectroscopy. Applied Sciences, 10(12), p.4345.

[85]Lima, R.B., Raza, R., Qin, H., Li, J., Lindström, M.E. and Zhu, B., 2013. Direct lignin fuel cell for power generation. RSC advances, 3(15), pp.5083-5089.

[86]Cao, X.; Ma, L.; Liang, Y.; Gao, B.; Harris, W. Simultaneous immobilization of lead and atrazine in contaminated soils using dairy-manure biochar. Environ. Sci. Technol. 2011, 45, 4884-4889.

[87]Joseph, S.D., B. J. et al., 2010. An investigation into the reactions of biochar in soil. Australian Journal of Soil Research, 48(6), pp.501-515.

[88]Oginni, O. and Singh, K., 2019. Pyrolysis characteristics of Arundo donax harvested from a reclaimed mine land. *Industrial Crops and Products*, *133*, pp.44-53.

[89]Essandoh, M., Wolgemuth, D., Pittman, C.U., Mohan, D. and Mlsna, T., 2017. Adsorption of metribuzin from aqueous solution using magnetic and nonmagnetic sustainable low-cost biochar adsorbents. Environmental Science and Pollution Research, 24, pp.4577-4590.

[90]European Certificate for a Sustainable Production of Biochar, 2015. pp. 1-21. doi: 10.13140/RG.2.1.4658.7043.

[91]International Biochar Initiative, 2015. Standardized product definition and product testing guidelines for biochar that is used in soil. International Biochar Initiative, p. 23. doi: 10.1016/j.zefq.2013.07.002.

[92]Suliman, W., Harsh, J.B., Abu-Lail, N.I., Fortuna, A.M., Dallmeyer, I. and Garcia-

Perez, M., 2016. Influence of feedstock source and pyrolysis temperature on biochar bulk and surface properties. Biomass and Bioenergy, 84, pp.37-48.

[93]Dhar, S.A., Sakib, T.U. and Hilary, L.N., 2022. Effects of pyrolysis temperature on production and physicochemical characterization of biochar derived from coconut fiber biomass through slow pyrolysis process. Biomass Conversion and Biorefinery, 12(7), pp.2631-2647.

[94]Devi, P. and Saroha, A.K., 2015. Effect of pyrolysis temperature on polycyclic aromatic hydrocarbons toxicity and sorption behaviour of biochars prepared by pyrolysis of paper mill effluent treatment plant sludge. Bioresource technology, 192, pp.312-320.

[95]Liu, R., Liu, G., Yousaf, B. and Abbas, Q., 2018. Operating conditions-induced changes in product yield and characteristics during thermal-conversion of peanut shell to biochar in relation to economic analysis. Journal of Cleaner Production, 193, pp.479-490.

[96]Lee, J.W., Kidder, M., Evans, B.R., Paik, S., Buchanan Iii, A.C., Garten, C.T. and Brown, R.C., 2010. Characterization of biochars produced from cornstovers for soil amendment. Environmental science & technology, 44(20), pp.7970-7974.

[97]Sharma, R.K., Wooten, J.B., Baliga, V.L., Lin, X., Chan, W.G. and Hajaligol, M.R., 2004. Characterization of chars from pyrolysis of lignin. Fuel, 83(11-12), pp.1469-1482.

[98]Onay, O., 2007. Influence of pyrolysis temperature and heating rate on the production of bio-oil and char from safflower seed by pyrolysis, using a well-swept fixed-bed reactor. Fuel processing technology, 88(5), pp.523-531.

[99]Yang, H., Huan, B., Chen, Y., Gao, Y., Li, J. and Chen, H., 2016. Biomass-based pyrolytic polygeneration system for bamboo industry waste: evolution of the char structure and the pyrolysis mechanism. Energy & Fuels, 30(8), pp.6430-6439.

[100]Wang, Q., Yue, Y., Liu, W., Liu, Q., Song, Y., Ge, C. and Ma, H., 2023. Removal performance of koh-modified biochar from tropical biomass on tetracycline and Cr (VI). Materials, 16(11), p.3994.

[101]Wu, Z., Wang, X., Yao, J., Zhan, S., Li, H., Zhang, J. and Qiu, Z., 2021. Synthesis of polyethyleneimine modified CoFe2O4-loaded porous biochar for selective adsorption properties towards dyes and exploration of interaction mechanisms. Separation and Purification Technology, 277, p.119474.

[102]Li, P., Zhao, T., Zhao, Z., Tang, H., Feng, W. and Zhang, Z., 2023. Biochar derived from Chinese herb medicine residues for rhodamine B dye adsorption. ACS omega,

8(5), pp.4813-4825.

[103]Sing, K.S., 1985. Reporting physisorption data for gas/solid systems with special reference to the determination of surface area and porosity (Recommendations 1984). Pure and applied chemistry, 57(4), pp.603-619.

[104]Wang, K., Lin, G., Meng, J., Guo, J., Tan, B., Liu, S., Lin, Q., Wu, X. and Gao, X., 2024. Textural properties prediction of KOH-activated carbon prepared from coal based on pyrolysis kinetics. Waste Disposal & Sustainable Energy, 6(4), pp.487-500.

[105]Sevilla, M., Fuertes, A.B. and Mokaya, R., 2011. High density hydrogen storage in superactivated carbons from hydrothermally carbonized renewable organic materials. Energy & Environmental Science, 4(4), pp.1400-1410.

[106]Rajapaksha, A.U., Chen, S.S., Tsang, D.C., Zhang, M., Vithanage, M., Mandal, S., Gao, B., Bolan, N.S. and Ok, Y.S., 2016. Engineered/designer biochar for contaminant removal/immobilization from soil and water: potential and implication of biochar modification. Chemosphere, 148, pp.276-291.

[107]Zhao, C., Ma, J., Li, Z., Xia, H., Liu, H. and Yang, Y., 2020. Highly enhanced adsorption performance of tetracycline antibiotics on KOH-activated biochar derived from reed plants. RSC advances, 10(9), pp.5066-5076.

[108]Vamvuka, D. and Sfakiotakis, S., 2011. Effects of heating rate and water leaching of perennial energy crops on pyrolysis characteristics and kinetics. Renewable Energy, 36(9), pp.2433-2439.

[109]Kumar, U., Maroufi, S., Rajarao, R., Mayyas, M., Mansuri, I., Joshi, R.K. and Sahajwalla, V., 2017. Cleaner production of iron by using waste macadamia biomass as a carbon resource. Journal of cleaner production, 158, pp.218-224.

[110]Qin, L., Wu, Y., Hou, Z. and Jiang, E., 2020. Influence of biomass components, temperature and pressure on the pyrolysis behavior and biochar properties of pine nut shells. Bioresource Technology, 313, p.123682.

[111]Chen, Y., Yang, H., Wang, X., Zhang, S. and Chen, H., 2012. Biomass-based pyrolytic polygeneration system on cotton stalk pyrolysis: influence of temperature. Bioresource technology, 107, pp.411-418.